

A simple circuit model of visual cortex explains neural and behavioral aspects of attention

Grace W. Lindsay^{a,*}, Daniel B. Rubin^{b,*}, Kenneth D. Miller^c

^a*Gatsby Computational Neuroscience Unit, Sainsbury Wellcome Centre, University College London, London, UK*

^b*Department of Neurology, Massachusetts General Hospital, Harvard Medical School, Boston MA*

^c*Center for Theoretical Neuroscience, College of Physicians and Surgeons, Mortimer B. Zuckerman Mind Brain Behaviour Institute, Swartz Program in Theoretical Neuroscience, Kavli Institute for Brain Science, New York, Department of Neuroscience, Columbia University, New York, United States*

Abstract

Selective visual attention modulates neural activity in the visual system and leads to enhanced performance on difficult visual tasks. Here, we use an existing circuit model of visual cortex, known as the stabilized supralinear network, to demonstrate that many neural correlates of attention can arise from simple circuit mechanisms. Using different variants of the model we replicate results from studies of both feature and spatial attention. In addition to firing rate changes, we also replicate findings regarding how attention impacts trial-to-trial variability. Finally, we expand this circuit model into an architecture that can perform visual tasks in order to show that these neural effects can enhance detection performance. This work advances our understanding of the physical underpinnings of attention.

Keywords: Attention, Normalization, Neural Networks

1. Introduction

2 When an animal knows in advance what features or locations in the visual
3 scene will be relevant for completing its goals, selective top-down attention

*These authors contributed equally to the work. Corresponding author: Grace W. Lindsay, gracewindsay@gmail.com

4 can be deployed. This attention has been shown to have a powerful modula-
5 tory effect on both task performance and neuronal responses, and changes in
6 the latter can often be powerful predictors of the former (Ress et al., 2000).

7 Numerous specific impacts of attention on neural activity have been iden-
8 tified, including changes in firing rates, trial-to-trial variability, and noise
9 correlations (Treue and Maunsell, 1999; Treue and Martinez Trujillo, 1999;
10 Cohen and Maunsell, 2009). Looking at the impact of attention on tuning
11 curves, attention to a preferred stimulus is known to scale up the responses
12 to all stimuli; conversely, attention to a non-preferred stimulus scales re-
13 sponses down (Martinez-Trujillo and Treue, 2004). This enhancement has
14 been shown to be a largely multiplicative increase in neuronal gain (Treue
15 and Martinez Trujillo, 1999). A similar percentage change occurs in the firing
16 rates of excitatory and inhibitory neurons (Mitchell et al., 2007).

17 Many of attention’s impacts on firing rates can be understood in the
18 context of the normalization model of attention (Reynolds and Heeger, 2009;
19 Lee and Maunsell, 2009; Ghose, 2009; Boynton, 2009). This model builds
20 off the canonical computation of normalization observed in multiple places
21 in the visual system as well as other brain areas (Carandini and Heeger,
22 2012). In the absence of attention, a neuron’s firing rate can be predicted
23 by a divisive normalization equation: stimuli with the preferred features and
24 in the classical receptive field of the neuron form the numerator (known as
25 the “stimulus drive”), and the denominator is a function of a less-selective
26 suppressive drive that includes surround locations and non-preferred features
27 as well. Under the normalization model of attention, attention provides a
28 biasing effect that amplifies the drive coming from the attended stimulus.

29 This model captures how attention can, when two stimuli are present,
30 shift responses to those of the attended stimulus alone. For example, when
31 a preferred and non-preferred stimulus are both presented to the receptive
32 field of a V4 neuron, the cell’s response is intermediate between the responses
33 evoked by each stimulus alone. By attending to either the preferred or non-
34 preferred stimulus, the response is shifted towards the response evoked by
35 the attended stimulus alone (Reynolds and Desimone, 2003). Similarly, at-
36 tention to a stimulus in the suppressive surround of a V4 neuron increases
37 the suppression induced, whereas attention to the center reduces the sup-
38 pression (Sundberg et al., 2009). The normalization model of attention also
39 captures how attention increases contrast gain or response gain, respectively,
40 depending on whether the attention is over a larger or smaller cortical area
41 than the stimulus input (Reynolds and Heeger, 2009).

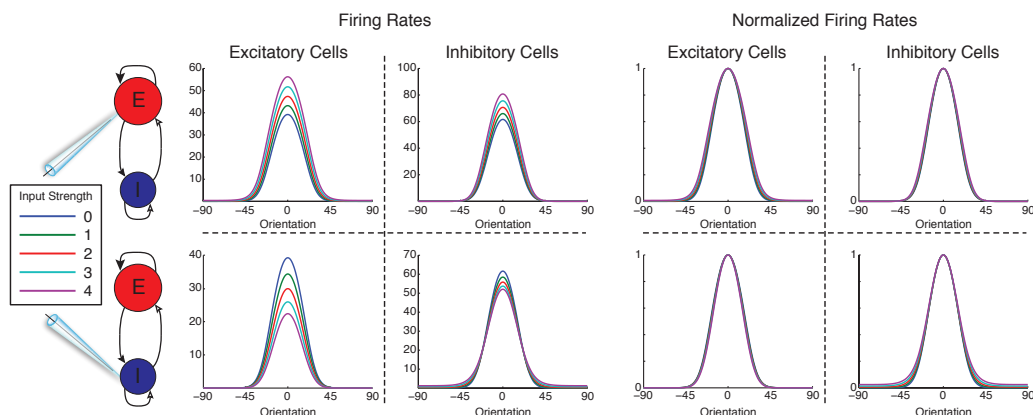


Figure 1:

Expansive nonlinearity and balanced amplification yield multiplicative scaling. We consider a simple two-unit nonlinear SSN model, with one excitatory (E) cell and one inhibitory (I) cell (Methods 4.1.4). We drove both cells with a series of feedforward inputs, whose strengths varied as a function of “orientation” to generate “tuning curves”. While driving the cells with this feedforward input, an additional constant input of one of four varying strengths (indicated by color legend at left) was added to either the E or the I cell. With increasing input to the E cell, both E and I rates are scaled up, whereas with increasing input to the I cells, both E and I rates are scaled down. Normalizing each curve by its maximum reveals that the gain change is almost exclusively multiplicative.

42 Beyond changes in firing rates described by the normalization model of
 43 attention, attention also decreases trial-to-trial variability and noise correla-
 44 tions across neuron pairs (Cohen and Maunsell, 2009; Mitchell et al., 2007).

45 We have previously shown that a simple model of cortical circuitry—
 46 known as the stabilized supralinear network (SSN) (Ahmadian et al., 2013)—
 47 can account for a wide set of phenomena described by the normalization
 48 model, including feature normalization and surround suppression and their
 49 nonlinear dependencies on contrast (Rubin et al., 2015). It also accounts
 50 for the suppression of correlated variability by a stimulus (Hennequin et al.,
 51 2018). The network assumes expansive or supralinear input/output functions
 52 for the individual units. As described in (Ahmadian et al., 2013; Rubin et al.,
 53 2015; Ahmadian and Miller, 2019), this causes effective synaptic strengths
 54 between units, which are proportional to the postsynaptic neuron’s gain —

55 its change in firing rate for a given change in input – to grow with increasing
56 postsynaptic activation. The growth of excitatory-to-excitatory effective con-
57 nections leads to potential instability, but with sufficiently strong feedback
58 inhibition the network remains stable. However, this stabilization occurs
59 through the network dynamically “loosely balancing” its inputs, so that the
60 recurrent input largely cancels the feedforward input, leaving a residual net
61 input that grows sublinearly as a function of the feedforward input. (The
62 balancing is “loose” because the residual input after cancellation is compa-
63 rable in size to the factors that cancel, Ahmadian and Miller, 2019.) This
64 cancellation of feedforward input through increasingly strong inhibitory sta-
65 bilization leads to the normalization and variability suppression effects just
66 described.

67 The SSN has strong recurrent excitation stabilized by strong feedback
68 inhibition and exhibits “balanced amplification” (Hennequin et al., 2018;
69 Murphy and Miller, 2009): small inputs biased toward either excitatory (or
70 inhibitory) cells drive large increases (or decreases) in both excitatory and
71 inhibitory firing rates. We hypothesized that attentional modulation acts
72 through the same balanced amplification and recurrent “loose balancing”
73 mechanisms that implement feature normalization and surround suppression.
74 Here we show that this model can indeed account for many of the neural
75 effects of attention observed in visual cortex.

76 Finally, in addition to replicating neural effects, we also use this model
77 to show how changes in neural activity can enhance performance. Previous
78 work (Lindsay and Miller, 2018) used a deep convolutional neural network
79 (CNN) as a model of the visual system to show how neural changes associated
80 with attention enhance performance on a challenging visual detection task.
81 Here, we put our circuit model into a convolutional architecture to create a
82 model that connects low-level circuitry with behavioral outputs. This model
83 (dubbed the SSN-CNN) replicates both the neural impacts of attention as
84 well as the performance enhancements.

85 **2. Results**

86 We employ four instantiations of our model of visual cortex to replicate
87 the neural effects of attention. The details of all of these models have been
88 described previously, and are included in the Methods section. All four mod-
89 els feature strongly recurrently connected excitatory and inhibitory neurons
90 with a supralinear neuronal input-output nonlinearity. The four models differ

91 only in the dimension of stimulus space over which the neurons are arranged
92 and the spatial arrangement and strengths of the connections between neu-
93 rons. In the simplest model, we consider a single pair of excitatory and
94 inhibitory neurons (Figure 1). The two slightly more complex models rep-
95 resent populations of neurons either arranged around a ring, with position
96 on the ring interpreted as preferred orientation of cells with a similar retino-
97 topic receptive field (RF) position (Methods 4.1.1, Figure 2), or on a line,
98 with position on the line interpreted as retinotopic RF position of cells with
99 similar preferred orientation (Methods 4.1.2, Figure 15). The most complex
100 model has a 2-dimensional representation of retinotopic space on which is
101 superimposed a map of preferred orientations. In this model, neurons make
102 connections as probabilistic functions of difference in stimulus preference over
103 the three dimensions of stimulus quality: two spatial dimensions and orien-
104 tation (Methods 4.1.3).

105 We note that the suppression of response to a preferred orientation by
106 simultaneous presentation of an orthogonal orientation or “mask” (“cross-
107 orientation suppression”) in V1 is largely mediated by nonlinear changes in
108 the pattern of thalamic firing induced by the mask, rather than by nonlinear
109 V1 integration (Priebe and Ferster, 2006; Li et al., 2006), although there is
110 a component mediated by V1 as shown by suppression arising when the two
111 stimuli are presented to different eyes (Sengpiel and Vorobyov, 2005). In our
112 models, the inputs to the model cortex are assumed to sum linearly, so that
113 all nonlinear behavior arises from cortical processing. We typically refer to
114 different competing stimuli presented within an RF as “orientations”, but this
115 should be understood to model cortical processing given linear summation
116 of inputs induced by two stimuli, rather than the literal phenomenon of V1
117 cross-orientation suppression.

118 In all instantiations, attention is modeled as a small additional excita-
119 tory input biased towards the excitatory cells within the specified locus of
120 attention. As a secondary test, we also re-ran all simulations with attention
121 instead modeled as a small inhibitory input towards the inhibitory cells (re-
122 sulting in a disinhibition of locally-connected excitatory cells). Results were
123 qualitatively similar, with a few notable exceptions discussed below.

124 To investigate the impact of neural activity changes on performance, we
125 also incorporated one of these circuit models—the ring model—into a con-
126 volutional neural network architecture (Methods 4.3). This allowed us to
127 demonstrate that the application of attention to our circuit model can in-
128 crease performance on a challenging visual detection task.

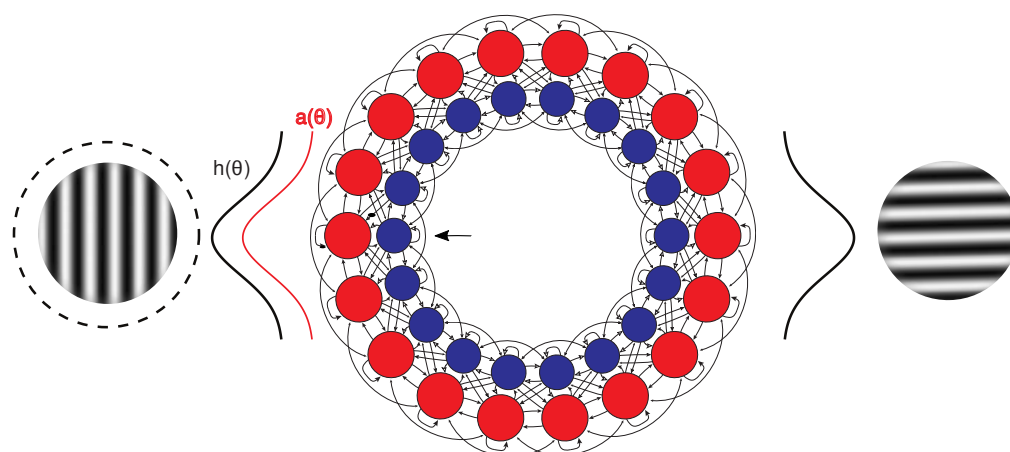


Figure 2:

A ring model of attention. The ring model represents different features (*e.g.*, preferred orientation) at a single location in visual space. At each location on the ring, a pair of excitatory (red) and inhibitory (blue) cells exist. Oriented stimuli are modeled as Gaussians centered at a particular location on the ring (black curves). Attention to one of the stimuli (indicated by dashed circle around it) is modeled as an additional Gaussian input biased towards the excitatory subpopulation at the center of the locus of attention (red curve). In this example, recording from the E-I pair indicated with the arrow would correspond to the cyan line in Figure 3.

129 2.1. Basic mechanism of the model

130 The balanced amplification model (Murphy and Miller, 2009) demon-
131 strates that in a network with strong recurrent connectivity, small changes
132 in the difference between E and I activity can drive large changes in the sum
133 of the activity. Previously, we have used this mechanism to produce models
134 of contextual modulation that capture the experimental observation that,
135 during surround suppression, both E and I firing rates are suppressed (Ozeki
136 et al., 2009). Within a locus of attention, however, the opposite effect is
137 observed: both E and I firing rates are enhanced (Mitchell et al., 2007).

138 In a network wherein neurons are described by a supralinear nonlinearity,
139 a bias in the input towards E or I shifts the responses of both cells up
140 or down (respectively), and the resulting change can be almost exclusively
141 multiplicative (Figure 1). Thus we hypothesize that this simple, intrinsic

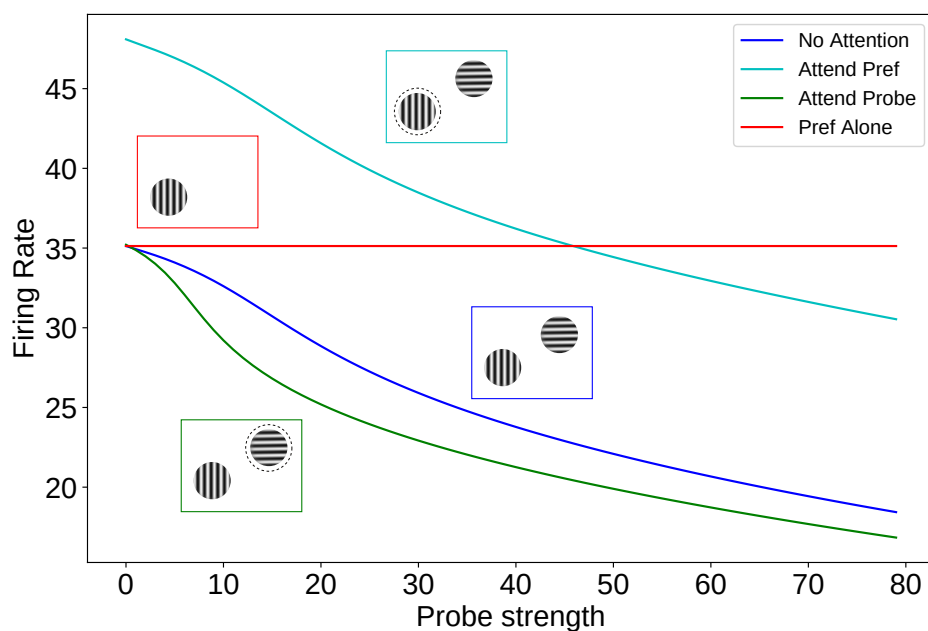


Figure 3:

Attention enhances the suppressive effect of non-preferred stimuli A stimulus of preferred orientation was shown to a cell in the ring model. An orthogonally oriented stimulus was presented along with the preferred stimulus, and the strength of the non-preferred “probe” was varied (blue line). The test was then repeated with attention (indicated by dashed circle around stimulus) directed towards either the preferred stimulus (cyan) or the probe stimulus (green). When attention was directed towards the preferred stimulus, suppression was decreased. When attention was directed to the probe stimulus, suppression was enhanced.

142 form of amplification may be sufficient to account for the observed effects
143 of attention on visual cortical circuits. We now incorporate this simple E-I
144 pair into a broader recurrent circuit and consider several recent experimental
145 results on attention in visual cortex.

146 2.2. Attention influences stimulus interactions

147 2.2.1. Impact of feature attention

148 In several regions of visual cortex, attention to one of multiple stimuli
149 presented within the receptive field of a neuron can shift the response of that

150 neuron towards the response evoked by the attended stimulus alone. This
151 was shown by Reynolds and Desimone (2003), who probed the responses of
152 V4 neurons with preferred and non-preferred stimuli, presented either alone
153 or together in the receptive field of a single neuron. They found that in the
154 simultaneous presentation condition, attending to a non-preferred stimulus
155 caused a relative suppression compared to an attend-away condition, whereas
156 attending to the preferred stimulus boosted the response. To simulate this
157 experiment, we recorded the response of a cell to a strong stimulus of preferred
158 orientation in the ring model (for details of attention experiments see
159 Methods 4.2). We then added a non-preferred stimulus at the orthogonal
160 orientation to the ring (schematized in Figure 2) and systematically varied
161 the strength of this “probe” stimulus. As expected, the addition of the non-
162 preferred probe was always suppressive, and with increasing probe strength
163 suppression was increased (Figure 3, blue line). We then repeated the same
164 test with attention directed either towards the preferred stimulus (cyan) or
165 the probe stimulus (green). When attention was directed towards the preferred
166 stimulus, the amount of suppression was decreased. When attention
167 was directed to the probe stimulus, suppression was enhanced.

168 In a related experiment, Treue and Martinez-Trujillo (1999) recorded from
169 a neuron in area MT while presenting two stimuli to the neuron’s receptive
170 field. One of the stimuli was always moving in a non-preferred direction,
171 while the direction of the other stimulus was systematically varied. Compared
172 to an attend-away condition, responses of MT neurons were relatively
173 suppressed at all stimulus directions when attention was directed towards
174 the non-preferred stimulus, but relatively enhanced when attending towards
175 the varying stimulus. We find the same result if we repeat this test in our
176 ring model (Figure 4). Like Treue and Martinez-Trujillo (1999), the change
177 we observe occurred without a substantial change in the width of tuning,
178 indicating a mainly multiplicative scaling (Figure 4, inset).

179 Note that in Figures 3 and 4 the same strength of attention is applied in
180 all circumstances, however attention applied to a non-preferred stimulus has
181 a weaker impact on firing rates. In our model, attention applied to a cell’s
182 preferred stimulus means additional excitatory inputs to the cell in question.
183 Attention to an orthogonal stimulus only impacts the recorded cell indirectly
184 through recurrent connections, leading to a weaker effect. Experimentally,
185 the magnitude of firing rate changes has been found to be weaker when
186 attention is applied to a non-preferred stimulus compared to a preferred one
187 (Treue and Maunsell, 1999).

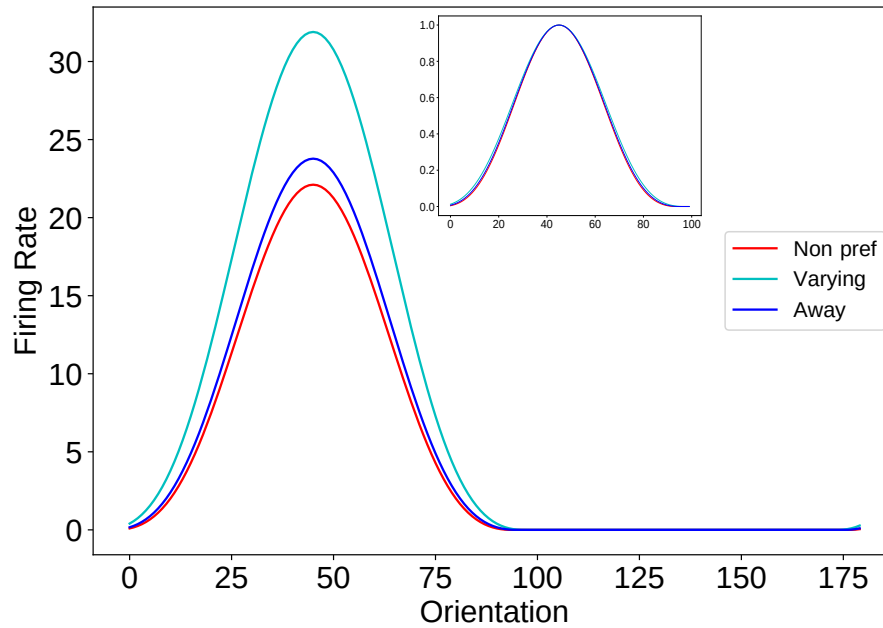


Figure 4:

Attention scales tuning multiplicatively. In the presence of a non-preferred probe stimulus, we varied the orientation of a test stimulus between 0° and 180° , while recording from the cell at 45° and attending either to the non-preferred probe (red), the varying stimulus (cyan), or away (blue). Attention produced an almost exclusively multiplicative change in response. Normalized responses are shown in the inset. There was virtually no change in tuning width, as observed experimentally (Treue and Martinez Trujillo, 1999).

188 *2.2.2. Correlation between feature attention and normalization*

189 Several groups have considered the mechanistic relationship between at-
190 tention and cortical normalization (Reynolds and Heeger, 2009; Lee and
191 Maunsell, 2009; Ni et al., 2012). In a recent study exploring the variabil-
192 ity in the strength of attentional modulation, Ni and colleagues demonstrated
193 that neurons vary in the degree to which their responses are normalized by
194 the presence of an orthogonal, non-preferred stimulus in the receptive field.
195 They further show that the degree of normalization a cell demonstrates (or
196 in their terminology, the broadness of the “tuning” of normalization – quan-
197 tified by a normalization modulation index) is highly correlated with the
198 extent to which attention modulates the response to the cell. To simulate
199 this experiment, we employed our 2-D model of visual cortex designed to
200 reproduce both the mean effects as well as a realistic degree of variability in
201 responses. In this simulation, excitatory cells were selected at random from
202 the population. For each cell, a high contrast stimulus of preferred orienta-
203 tion was presented. An orthogonal stimulus of the same size, position, and
204 strength (the “null” stimulus) was then presented, and then the preferred
205 and orthogonal stimuli were presented together. The firing rate response
206 in each of the three stimulus conditions was recorded, and the Normaliza-
207 tion Modulation Index was calculated as: $NMI = [(r(\text{Preferred}) - r(\text{Null})) -$
208 $(r(\text{Both}) - r(\text{Null}))] / [(r(\text{Preferred}) - r(\text{Null})) + (r(\text{Both}) - r(\text{Null}))]$. An NMI
209 of 0.33 corresponds to averaging of the two stimuli, whereas an NMI of 0
210 is considered a “winner take all” response (the response to the pair is the
211 same as the response to the preferred stimulus alone). In the terminology of
212 Ni et al., cells with highly tuned normalization have an NMI closer to 0 (Ni
213 et al., 2012). The paired presentations were then repeated (showing both
214 preferred + null together) with attention directed towards either the pre-
215 ferred or null stimulus. Attention was applied to the E cells in the position,
216 size, and orientation of either the preferred or null stimulus. An Attentional
217 Modulation Index was then calculated as: $AMI = (r(\text{Attend Preferred}) -$
218 $r(\text{Attend Null})) / (r(\text{Attend Preferred}) + r(\text{Attend Null}))$. As was observed
219 experimentally, there is a wide range of NMIs and AMIs, and the NMI and
220 AMI of cells are highly correlated (Figure 5).

221 *2.2.3. Impact of spatial attention*

222 The previously discussed experiments studied the response of neurons
223 to pairs of stimuli presented within the same receptive field. However, at-
224 tention has also been shown to modulate the effect of stimuli presented in

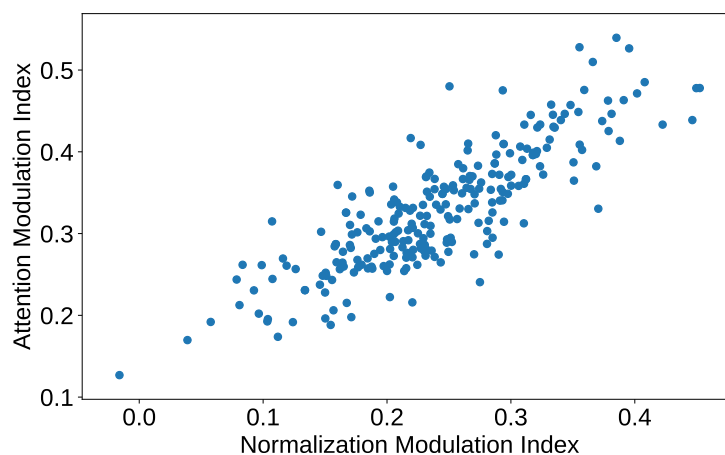


Figure 5: **Normalization strength and attentional modulation are positively correlated.** Normalization Modulation Indices are plotted against the Attention Modulation Indices for all 250 cells sampled from the 2-D model. Correlation coefficient: 0.84. See text for details.

225 the receptive field surround. Sundberg et al. (2009) found that in V4, the
226 strength of surround suppression could be either increased or decreased by
227 attending specifically to the surround or center stimulus. To simulate this
228 experiment, we next employed our line model used to simulate spatial contextual
229 interactions. Pairs of E and I cells are arranged along a one-dimensional
230 lattice representing an axis of retinotopic space, with recurrent excitatory
231 connections that decrease as a function of retinotopic/cortical distance. It is
232 assumed that the cells share preferred features. A stimulus was presented to
233 the cell in the center of the lattice, in the presence of a suppressive surround
234 stimulus. Attention was then directed to either the center or surround stimu-
235 lus. Attention to the center decreased the strength of surround suppression
236 (pushing firing rates towards those when the stimulus is presented alone),
237 while attention to the surround enhanced surround suppression (Figure 6).

238 We simulated this experiment in the 2-D model as well. 100 neurons
239 were randomly selected from the network. For each neuron, we measured
240 the response to a strong stimulus of preferred orientation centered on the
241 receptive field, and then added a strong stimulus of the same orientation
242 to the surround. The response to the cell was measured in the absence

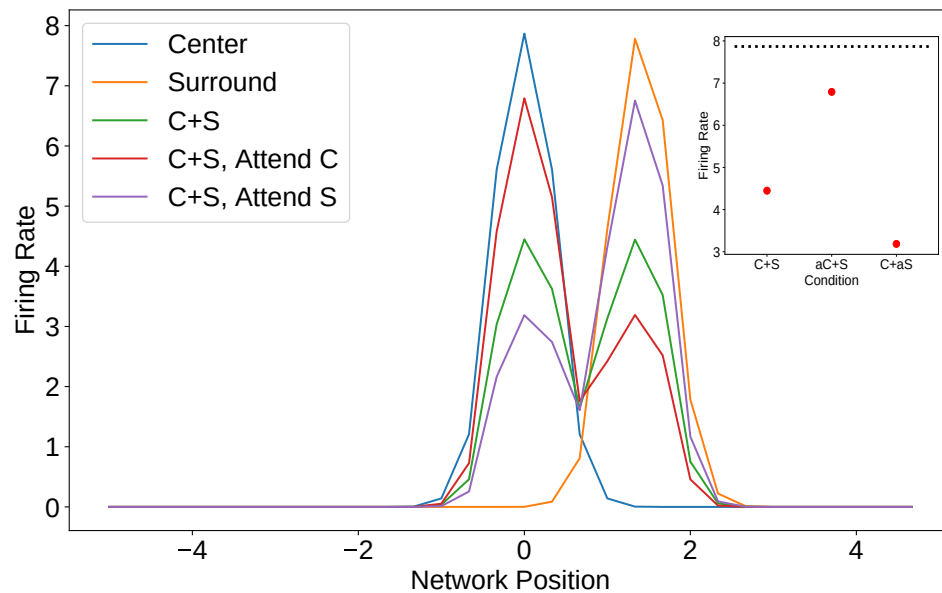


Figure 6:

Attention modulates the strength of surround suppression. A stimulus was shown in the receptive field of the neuron at position 0. A stimulus of equal strength and size was then placed in the surround, and the response was recorded from neurons in the vicinity. Attention was then directed either to the center or surround stimulus. In the main figure, the E cell activity across the network is shown in response to the center stimulus alone, the surround stimulus alone, the center and surround stimuli shown together, the center and surround stimuli with attention directed towards the center, and the center and surround stimuli with attention directed towards the surround. The inset demonstrates the activity at the center E cell – the dashed line is the response to the center stimulus alone, and the three dots show the response to the center and surround presented together, either with no attention, with attention directed towards the center, or with attention directed towards the surround.

243 of an attentional input (the “Attend Away” condition), as well as with an
244 attentional input directed towards the center or surround stimulus. As was
245 observed experimentally, attending to the surround boosted the amount of
246 surround suppression, whereas attending to the center greatly weakened the

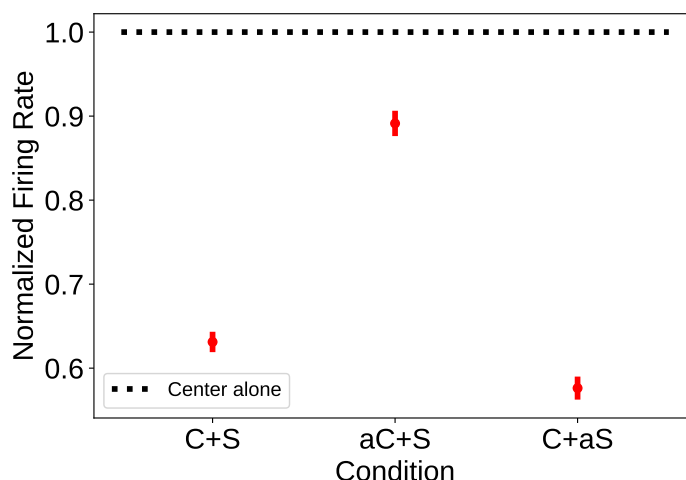


Figure 7:

Attention modulates the strength of surround suppression in the large scale model. A stimulus of preferred orientation was shown to a randomly selected cell. A stimulus with the same orientation and strength was placed in the surround, and the response was recorded. Attention was then directed either to the center or surround stimulus. The mean responses relative to the center alone is shown for a sample of 100 neurons from the 2-D model. Error bars indicate the standard error of the mean. All three response groups are significantly different from each other at $p < .005$ (student's t-test).

247 surround suppression (Figure 7, compare the results of the 2-D model to the
248 inset of Figure 6).

249 2.3. Experimental paradigm alters the impact of attention

250 2.3.1. Effect on contrast and response gain

251 All of the experiments and simulations discussed thus far demonstrate
252 that attention produces a gain change in the firing rate of neurons within the
253 locus of attention. The quality of this gain change, however, can be strongly
254 influenced by the relative sizes of the stimulus and the attentional field.
255 Reynolds and Heeger (2009) (their Figure 3) found in their normalization
256 model of attention that when attention is directed to a relatively large area,
257 the effect on the response to a small stimulus should be predominantly a
258 change in “contrast-gain”, such that cells respond to stimuli as if they were
259 effectively at higher contrast. This would be seen as a leftward shift in a

260 contrast-response curve for a stimulus, with relatively little change in the
261 maximum firing rate. For a large stimulus and a small attentional field, they
262 instead predict a change in “response-gain”, such that all responses are scaled
263 multiplicatively.

264 Here we again employ the one-dimensional spatial line network model
265 to study the two different effects of attention described by Reynolds and
266 Heeger (2009). Attention was still modeled as a small additional input only
267 to excitatory cells over a defined spatial area, and we calculated “contrast
268 response curves” with and without attention. (Note that what we call “con-
269 trast” is actually external input strength, *i.e.* the parameter c in Eq. 3; in
270 reality, external input strength, as measured by thalamic input firing rate,
271 is a monotonic but nonlinear, saturating function of stimulus contrast, (*e.g.*
272 Sclar, 1987; Sclar et al., 1990).) To quantify changes in the contrast response
273 properties, we fit each curve to a standard Naka-Rushton equation (Naka
274 and Rushton, 1966):

$$R(c) = R_{max} \left(\frac{c^n}{c_{50}^n + c^n} \right) \quad (1)$$

275 where R_{max} is the plateau firing rate, n describes the steepness of the contrast
276 response curve, and c_{50} is the strength of the stimulus at which the response is
277 50% of its maximum. In our fitting procedure, the value of n is discovered for
278 the no-attention condition, and held at that value when fitting the attended
279 condition.

280 With a large attentional field and small stimulus, the effect of atten-
281 tion was predominantly a leftward shift in the contrast-response function,
282 as predicted by the model of Reynolds and Heeger (2009). We quantified
283 this change in “contrast gain” as the difference in the c_{50} parameters of the
284 contrast response curves produced with and without attention (Figure 8A).
285 We compared this to the “response gain”, which we quantify as the ratio
286 of R_{max} parameters with and without attention. With a large stimulus and
287 small attentional field, the effect of attention was reversed: there was little
288 change in the contrast gain, and a much larger change in the response gain
289 (Figure 8B). The dashed lines in either figure show the percent change in
290 firing rate induced by attention. With a change in contrast gain there is
291 little change in firing at the largest contrast, but this is not true for a change
292 in response gain.

293 While Reynolds and Heeger (2009) showed this property in their descrip-
294 tive model of attention, conditions that produce changes in contrast or re-

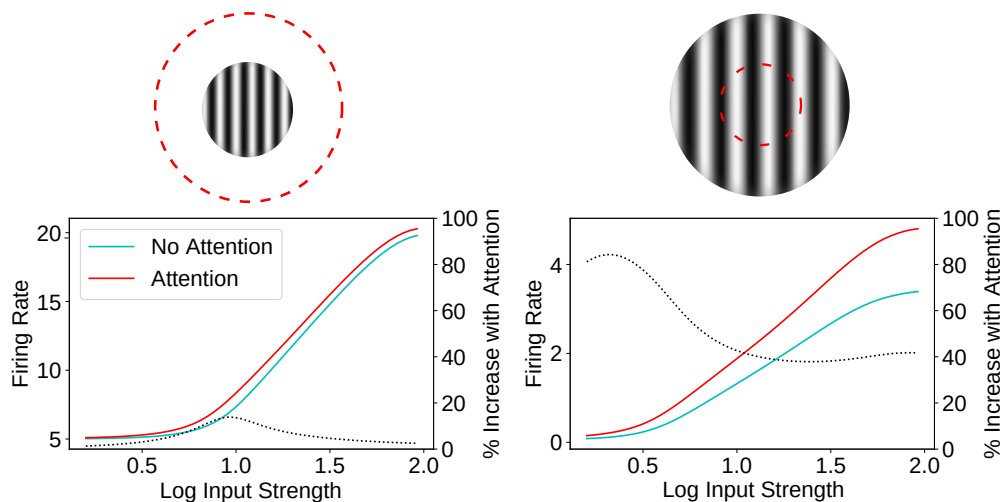


Figure 8:

The qualitative effect of attention depends on the relative sizes of the attentional and stimulus fields. Here we used the spatial line model to study the two different effects of attention, as described by Reynolds and Heeger (2009), Figure 3. Contrast response curves were calculated by varying the input strength logarithmically (base 10) in the presence (red curves) and absence (cyan curves) of attention. Left: with a large attentional field (red dashed circle) and small stimulus, the impact of attention was largely on contrast gain, defined as the difference between c_{50} values with and without attention (R_{max} ratio: 0.98, c_{50} difference: -6.43). Right: in the “small attentional field, large stimulus” condition, attention mainly affected response gain, defined as the ratio of R_{max} values (R_{max} ratio: 1.39, c_{50} difference: -0.88). Dotted lines show the percent change in firing caused by attention.

295 sponse gain have also been shown experimentally. Martinez-Trujillo and
296 Treue (2002) recorded from neurons in area MT while presenting two stimuli
297 within the receptive field. One stimulus was moving in a preferred direction,
298 and the other in a non-preferred direction. They then varied the strength of
299 the preferred stimulus while holding the contrast of the non-preferred stim-
300 ulus fixed, and directed the monkey to attend either to the non-preferred
301 stimulus or outside of the receptive field. They found that attending to
302 the non-preferred stimulus caused predominantly a change in contrast-gain.

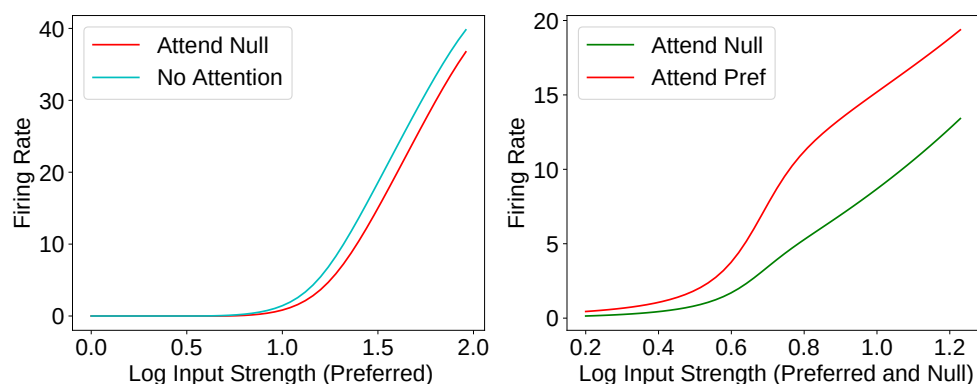


Figure 9:

Experimental paradigm alters gain change type. A. In the ring model, in the presence of a fixed-strength non-preferred stimulus, the contrast of a preferred stimulus was varied logarithmically (base 10) while attention was directed either away (cyan) or towards the non-preferred stimulus (red) as in Figure 4 of Reynolds and Heeger (2009). Attention to the non-preferred stimulus produced mainly a reduction in contrast gain, measured as the difference between c_{50} values (R_{max} ratio: .97, c_{50} difference: 5.94) (Martinez-Trujillo and Treue, 2002). **B.** Showing preferred and non-preferred stimuli of equal but varying contrast while attending to one or the other produced a much larger change in response gain, measured as the R_{max} ratio (R_{max} ratio: 1.38, c_{50} difference: -2.17). This was studied experimentally in Lee and Maunsell (2009).

303 However, Lee and Maunsell showed that if the contrast of both the preferred
304 and non-preferred stimulus were varied simultaneously, attending to one or
305 the other stimulus would produce a much larger change in response gain (Lee
306 and Maunsell, 2009). Using the ring model again, we modeled both of these
307 stimulus conditions, and find analogous results (Figure 9A, B).

308 2.3.2. Effect on length tuning

309 The impact of spatial attention on length tuning was explored in Roberts
310 et al. (2007). In this study, the length of an oriented bar was varied as firing
311 rates from V1 cells were recorded. Attention was directed to the stimulus or
312 to a stimulus in the opposite hemifield. The authors found that, for receptive
313 fields near the fovea, attention had the effect of decreasing preferred length

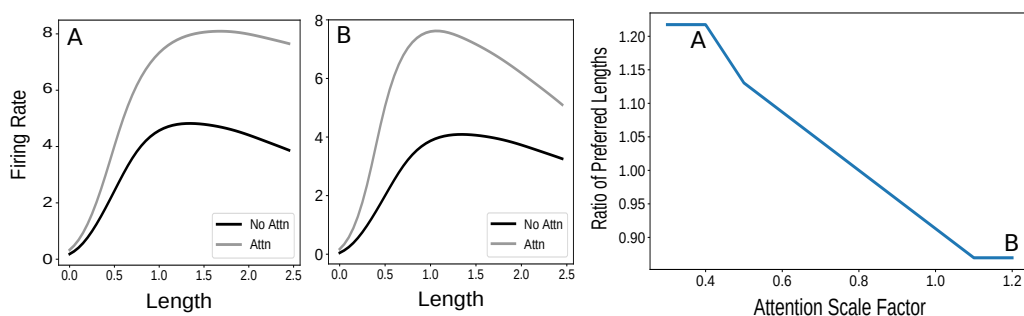


Figure 10:

Size of attention influences length tuning. Using the line model, we presented a stimulus of increasing length (left two plots). If attention was small compared to the stimulus (far left) attention shifted the preferred length (i.e., the length that elicits the highest firing rate) rightward, making it larger. If the area to which attention was applied was large compared to the stimulus (middle), the opposite occurred. Thus, varying the ratio of the size of attention to the stimulus size (“attention scale factor”) caused a shift in the ratio of the preferred lengths (preferred length with attention divided by preferred length without attention; right plot). Scale factor in the far left plot is marked on the right plot by the letter A, middle by B. In Roberts et al. (2007) the ratio of preferred lengths for parafoveal receptive fields was .88 and for peripheral receptive fields 1.19.

314 (that is, the length of the bar that elicits the highest firing rate). For receptive
315 fields in the periphery, the reverse was true: attention increased the preferred
316 length.

317 We explored attention’s impact on length tuning using the spatial line
318 model. For different lengths of the stimulus, firing rates were recorded from
319 a neuron at the center. The effect of attention varied as a function of the size
320 of the attentional field. In Figure 10 (right) the ratio of the size of attention
321 to the size of the stimulus is on the x-axis. By keeping a fixed ratio of attention
322 size to stimulus size, we assume that the size of the attentional field scales
323 with the size of the stimulus, but this scaling factor may differ for different
324 cells. For small values of this attention scale factor, the preferred length with
325 attention was greater than the preferred length without it. For higher values,
326 this ratio was reversed. Firing rate as a function of length for two different
327 values of the attention scale factor are shown on the left. This pattern of

328 how attention impacts preferred lengths reflects the impact of attending to
329 the suppressive surround. With attention larger than the stimulus, more of
330 the suppressive surround is activated for any given stimulus length. This
331 effectively increases the length of the stimulus, making the preferred length
332 smaller than without attention.

333 Our results combined with the findings of Roberts et al. (2007) suggest
334 that attention targets parafoveal receptive fields differently than it targets
335 peripheral ones. In particular, spatial attention inputs to parafoveal cells
336 may be larger than the size of the stimuli these cells respond to. In the
337 periphery, spatial attention inputs may represent an area smaller than the
338 stimuli. This could be a result of the differently sized receptive fields in these
339 two regions.

340 *2.3.3. Factors influencing the magnitude of attentional effects*

341 In Lee and Maunsell (2010), the authors controlled attention and task dif-
342 ficulty across stimulus conditions while varying the number of stimuli in the
343 receptive field of MT neurons. Through this, they showed that attentional
344 modulation is weaker when only one stimulus is present in the receptive field,
345 and that this result is well-captured by a divisive normalization model. We
346 use the ring model to replicate these results. By presenting three different
347 stimuli (a most-, moderately-, and least-preferred orientation) either alone
348 or in pairs (Figure 11, left; compare to Lee and Maunsell (2010) Figure 4),
349 we show that the effect of an attentional input was strongest when applied
350 to one stimulus in a pair. In particular, effects of attention on firing rates
351 were highest when moving attention from outside the receptive field to the
352 preferred stimulus inside the receptive field when a non-preferred stimulus is
353 also present (Figure 11, right). The next strongest effect was from moving
354 attention from the non-preferred stimulus in the receptive field to the pre-
355 ferred. Finally, attention effects were weakest when moving attention from
356 outside the receptive field to a preferred stimulus presented alone inside the
357 receptive field.

358 A similar comparison was done using spatial attention rather than feature
359 attention in Sundberg et al. (2009). Here, attention was moved between the
360 receptive field center and the suppressive surround. A stimulus of preferred
361 orientation was present in the center and was present or absent in the sur-
362 round. The impact of attending the center was larger when the stimulus in
363 the surround was present (Figure 2 of Sundberg et al. (2009)). We replicated
364 these results using the line model. The firing rate of an excitatory cell was

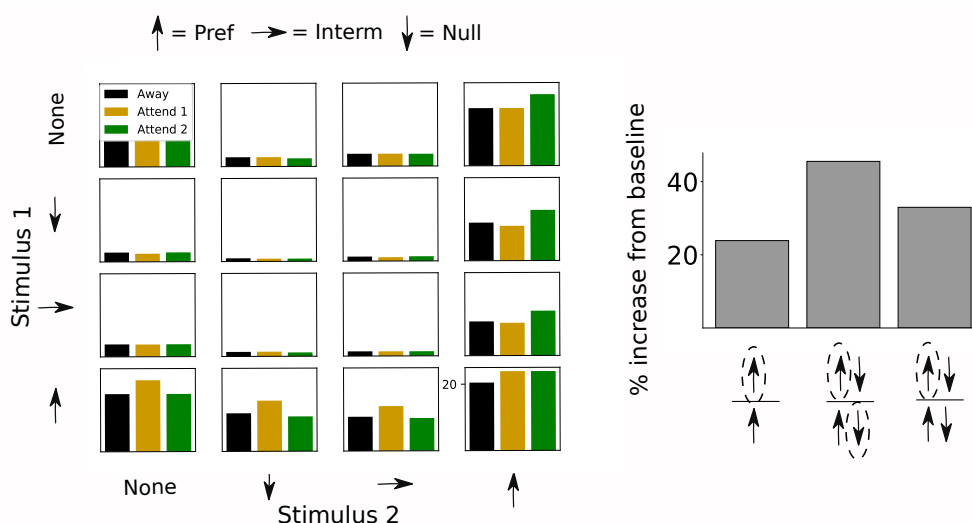


Figure 11:

Effects of attention are greater with more than one stimulus in the receptive field. Using the ring model, three different stimuli (preferred, intermediate, and null) were shown either individually or in pairs. Attention was directed to either of the two stimuli ('Attend 1' or 'Attend 2') or outside of the receptive field ('Away'; when only one stimulus was present, attending to the opposite stimulus is the same as attending away). Left: Bar plots represent steady state firing of the recorded neuron for all stimulus and attention conditions. Right: bar plots indicate percent increase in firing rate with attention, for three different comparisons. Arrows indicate which stimuli were in the receptive field for the two conditions being compared (bottom arrows indicate baseline condition, top arrow(s) indicate attended condition) and dashed circles indicate attended stimulus. The comparable values for these conditions from Lee and Maunsell (2010) are 9%, 59%, 28% respectively.

365 recorded with a stimulus centered on its preferred location. Attention was
 366 applied to this location, or to a location in the surround both in the presence
 367 and absence of a stimulus there. There results of this are shown in Figure 12
 368 (left).

369 In Sundberg et al. (2009), the impact of attention on surround suppression
 370 was also shown over time. The extent to which firing rates are decreased by
 371 the presence of the surround was measured when attention was directed to

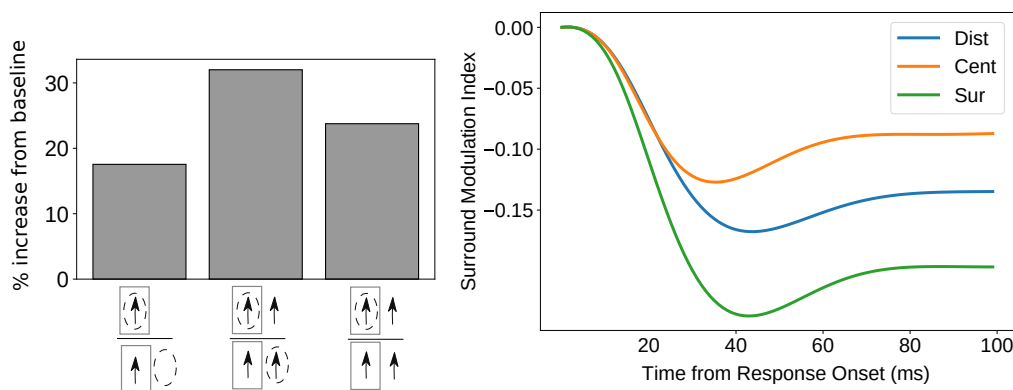


Figure 12:

Effects of attention are greater with a stimulus in the surround. Using the line model, a preferred stimulus was presented in the receptive field center. Left: bar plot indicates increase in firing in preferred-attended condition (top arrows) vs. baseline condition (bottom arrows). Rectangles indicate receptive field. The presence of a surround stimulus is indicated by an additional arrow outside the receptive field and attention is indicated by a dashed circle. The increase in firing was smaller without the surround present (comparable values from Sundberg et al. (2009) are 18.8% versus 36.8%. The authors do not report the percent increase compared to a baseline condition without attention to either center or surround). Right: the strength of firing rate modulation from the addition of a surround stimulus (the surround modulation index: $[r(C + S) - r(C)]/[r(C + S) + r(C)]$) is plotted vs. time, for different attention conditions: attending the surround, attending the center, and attending a distant location (modeled as no attention). The difference between these conditions emerged over time.

372 the receptive field center, surround, or to a distant location. The authors
373 note (their Figure 5) that the difference in surround modulation between
374 these different attention conditions emerged over time. The model shows the
375 same result (Figure 12, right). The differences emerge faster in our model
376 than in the data (in the data, the difference is not seen in the time bin 15-
377 55ms after response onset, but emerges sometime in the next 40ms time bin).
378 However, our model does not take into account any delays in the onset of the
379 attentional signal relative to the onset of stimulus-driven feedforward input
380 to the recorded neurons.

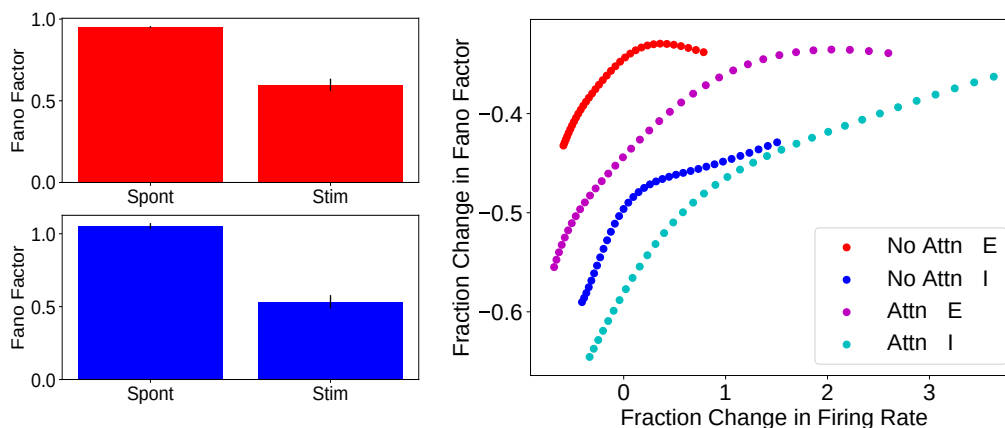


Figure 13:

Attention causes a reduction in trial-to-trial variability. In the ring model with noisy background input, 35 E (red) and 35 I (blue) cells were recorded as a stimulus that was oblique (but not orthogonal) to their preferred stimuli was presented. Stimulus onset produced a substantial reduction in trial-to-trial variability, measured as the Fano factor, compared to spontaneous activity (left; errorbars are STD). Next, the effect of an attentional modulation was observed. On the right, fractional change in Fano factor is plotted as a function of fractional change in firing rate for each of the 35 E and 35 I cells in the presence and absence of attention. In all cells, stimulus onset produced a decrease in the trial-to-trial variability, regardless of whether the stimulus produced an increase, decrease, or no change in the mean firing rate (Churchland et al., 2010). In the presence of attention, this decrease in variability was enhanced, as has been observed experimentally (Mitchell et al., 2007). The percent change in both firing rate and Fano factor was calculated for each cell by taking a time average of both the mean rate and Fano factor before and after the onset of the stimulus (in trials with attention, it came on at the same time as the stimulus).

381 *2.4. Attention reduces trial-to-trial variability and noise correlations*

382 In addition to its effects on mean firing rates, attention has also been
383 shown to modulate the variability in rates across trials. Mitchell et al. (2007)
384 showed that attending to a stimulus decreased the across-trial variability of

385 neural responses when compared to trials in which attention was directed
386 elsewhere. Furthermore, this experiment showed that this decrease in vari-
387 ability occurs in both broad spiking (putative excitatory) cells and narrow
388 spiking (putative inhibitory) cells.

389 To study this effect in our model, we introduced a source of trial-to-trial
390 variability into our ring network by given each neuron a noisy input in addi-
391 tion to its stimulus inputs, similarly to Hennequin et al. (2018) (see Methods
392 4.1.1 for details). We then ran 1,000 trials of a simple stimulus presentation.
393 On half of these trials, attention was directed towards the stimulus being
394 presented. On the other half there was no attentional modulation added to
395 the network. The stimulus onset produced a reduction in the trial-to-trial
396 variability, measured as the Fano factor, with this reduction occurring both
397 for neurons that are activated by the stimulus and neurons that are not acti-
398 vated or suppressed (Figure 13), as in experiments (Churchland et al., 2010)
399 and as previously shown for the SSN (Hennequin et al., 2018). Addition
400 of attention caused an additional drop in Fano factor, again regardless of
401 whether the stimulus plus attention caused a net increase, zero change, or
402 net decrease in firing rate (Figure 13, right).

403 In addition to causing a drop in trial-to-trial variability, Cohen and col-
404 leagues demonstrated that an even stronger effect of attention on network
405 variability is a pronounced decrease in the magnitude of noise correlations
406 between neurons in V4 (Cohen and Maunsell, 2009). This aligns with the
407 finding that a stimulus suppresses the shared or correlated component of
408 neural variability, not the component private to each neuron (Churchland
409 et al., 2010). Cohen *et al.*, 2009, recorded from thousands of pairs of neu-
410 rons and multiunit clusters in V4 during a visual change detection task, and
411 found that the presence of attention greatly enhanced performance. They
412 further showed that the significant improvement in performance was not due
413 to changes in single neurons, but rather to a pronounced drop in the corre-
414 e correlations). To simulate this experiment, we recorded from pairs
415 of excitatory cells in the ring model in the presence of noisy input while
416 presenting the network with two high-contrast oblique stimuli. On half of
417 the trials, attention was directed to one of the stimuli. We calculated the
418 correlation between all pairs of recorded neurons in the presence and absence
419 of attention. Pairs of neurons were grouped based on their distance from each
420 other on the ring (i.e. difference in preferred orientation). The changes in
421 firing for two example neurons with attention as well as the noise correlations
422 between them over the course of an example trial are shown in Figure 14

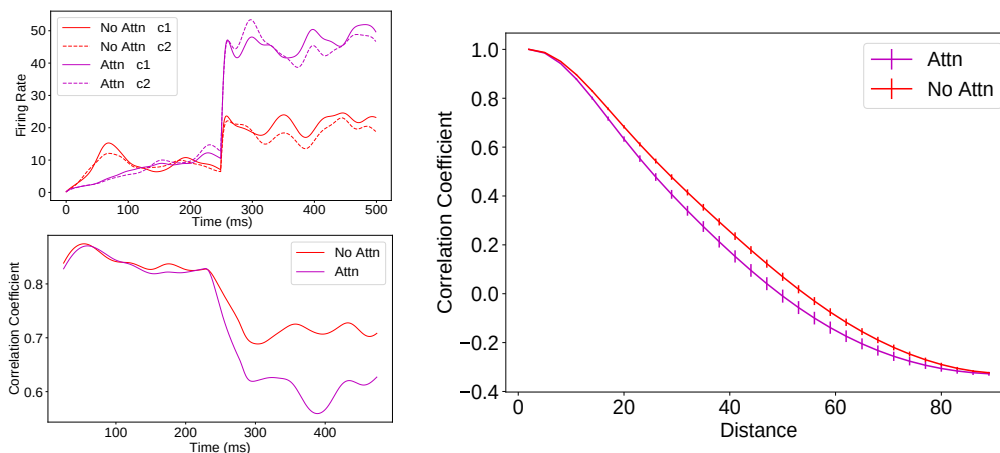


Figure 14:

Attention decreases noise correlations between neurons. In the ring model with noisy background input, stimulus onset produced a reduction in noise correlations between pairs of neurons in the network. The correlation in firing rates between each pair of cells was calculated as a function of time for each of the two conditions. On the left, an example pair is shown. The mean firing rates of two excitatory cells in each of the two conditions is plotted on top; stimulus (at 90 degrees) and attention turn on at 250ms. The correlations between the two cells are plotted on the bottom. Correlation time-series are shown as a running average with a 50-ms sliding window. On the right, the mean correlation between pairs of recorded cells (representing 30-65 degrees) during the stimulus response epoch is plotted against distance in preferred orientation. Error bars indicate SEM.

423 (left). The average value of noise correlations between neurons at various
424 distances is shown on the right. As was observed experimentally, attention
425 caused a reduction in the noise correlations between neurons beyond the
426 reduction caused by the stimulus alone.

427 The suppression of correlated variability can be understood as resulting
428 from the normalization performed by the model (although it also explains
429 further aspects of this suppression not explained simply by normalization,
430 Hennequin et al. (2018)). In particular, as has been observed experimen-
431 tally (Busse et al., 2009), this normalization averages the responses to ap-
432 proximately equal strength inputs but performs a more unequal averaging

433 of unequal strength stimuli, becoming “winner-take-all” when inputs differ
434 sufficiently in strength (Rubin et al., 2015). The reduction in correlated vari-
435 ability with increasing stimulus strength can be understood to occur because
436 the ongoing noisy inputs become steadily weaker relative to the stimulus.
437 The normalization thus increasingly favors the response to the stimulus and
438 suppresses the noise. Because this suppression is mediated by the network,
439 it acts on the correlated component of the noise and not on the private noise,
440 which is largely averaged out in its impact at the network level.

441 An alternative picture of the mechanism of suppression is that it oc-
442 curs through the enhancement of the strength of feedback inhibition with
443 increasing network activation (Hennequin et al., 2018). In particular, in
444 linearizations about the deterministic fixed point, the real parts of the lead-
445 ing eigenvalues become more negative with increasing mean stimulus drive,
446 representing increased feedback inhibition of the corresponding eigenvector
447 activity patterns onto themselves, dampening their fluctuations. Given struc-
448 tured connectivity, these activity patterns have similar structure and so their
449 fluctuations represent correlated variability.

450 Investigations regarding noise correlations have indicated that a decrease
451 in correlation with attention should only occur for pairs of neurons that repre-
452 sent the same stimulus whereas pairs of neurons representing different spatial
453 locations or features may actually see an increase in correlations (Averbeck
454 et al., 2006). This bi-directional effect of attention was found in area V4 (Ruff
455 and Cohen, 2014). In our ring model, this result occasionally occurred when
456 using weaker stimuli and/or a smaller number of trials to calculate the cor-
457 relations in the ring model. Examples of this can be found in Supplementary
458 Figure A.17.

459 The task in Ruff and Cohen (2014), however, used spatial rather than
460 feature attention. Specifically, subjects were required to perform a contrast
461 discrimination task in the cued hemifield. To replicate this study directly
462 we used the line model with two nearby stimuli of unequal contrast (Figure
463 15, left). The TTS metric from Ruff and Cohen (2014) measures the extent
464 to which a pair of cells have the same (positive TTS) or opposite (negative
465 TTS) preferred stimulus of the two presented. Replicating figure 5 from that
466 paper, we see that attention decreased correlations for cells with the same
467 preferred stimulus but increased it for those with opposite preferred stimuli
468 (Figure 15, right).

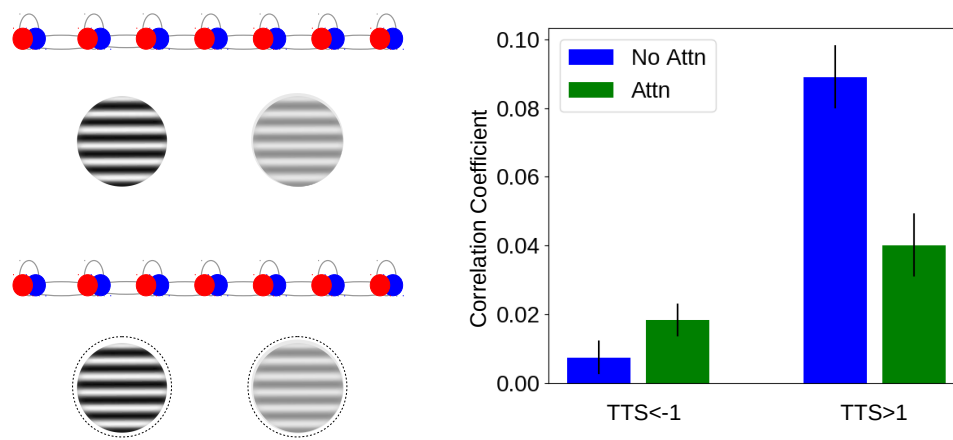


Figure 15:

Attention increases or decreases noise correlations between neurons based on preferred stimulus. In Ruff and Cohen (2014), animals performed a contrast discrimination task on two nearby stimuli, represented here as two inputs to the line model of different strengths. During different blocks, attention was directed to one of two such sets of stimuli, one in each hemifield. Here we model attention to the opposite hemifield as a 'no attention' condition (top left) and attention to the hemifield of the recorded cells as attention to each of the two stimuli simultaneously (bottom left). The 25 model cells we analyzed responded to one or the other stimulus alone. TTS values are the product of d-primes and represent whether a pair of cells has the same (positive) or different stimulus preference (negative). By creating 20 populations of 25 cells each, we analyzed the relationship between TTS and the effect of correlation on attention for 6000 cell pairs. Through this we found both a significant ($p \ll .05$) decrease in correlation with attention for cells that preferred the same stimulus and increase for cells that had opposite preferences (right). Error bars indicate SEM. For more details, see Methods 4.2.

469 2.5. An alternative mechanism

470 In all of the simulation results presented thus far, attentional modulation
471 has been modeled as a small excitatory input biased towards the excitatory
472 cells within the locus of attention. Here we consider instead a small in-

473 inhibitory input to inhibitory cells within the locus of attention, disinhibiting
474 rather than exciting the excitatory cells. This is motivated by two observa-
475 tions. First, it was observed that inputs from Anterior Cingulate Cortex to
476 V1 target the VIP class of inhibitory cells (Zhang et al., 2014). The VIP cells
477 in turn are known to inhibit other inhibitory neurons and, at least in V1,
478 disinhibit excitatory cells (*e.g.* Fu et al., 2014). The ACC input conceivably
479 could be involved in attentional modulation. Second, recent electrophysio-
480 logic work has revealed the function of two classes of inhibitory cells in layer
481 1 of cortex (Jiang et al., 2013). One of these classes, the single bouquet
482 cells (SBCs) was shown to preferentially inhibit the interneurons of deeper
483 layers, and so have a net disinhibitory effect on the local pyramidal cells. As
484 layer 1 receives a significant portion of its input from higher cortical areas,
485 it has been suggested that this circuit may play a role in attention and other
486 top-down modulation of local circuit activity (Larkum, 2013).

487 To test the feasibility of this mechanism in our model, we repeated our
488 suite of simulations using this alternative, disinhibitory mechanism of at-
489 tention. Rather than modeling attention as an additional excitatory input
490 to E cells, we instead model it as an additional inhibitory input to I cells.
491 The results of these simulations are presented in the Supplementary Figures.
492 Overall, this alternative mechanism can qualitatively reproduce most of the
493 findings we report above (Supplementary Figure A.18). Frequently, however,
494 the same value of the attention strength parameter produces weaker effects
495 on neural firing than when attention is directed towards the excitatory cells
496 (for example, compare Figure 12 to Figure A.18G).

497 In addition, there are instances where this form of attention does not
498 qualitatively replicate our original findings (Supplementary Figure A.19).
499 One major discrepancy between results comes from the use of the 2-D model.
500 Comparing Supplementary Figure A.19B to Figure 5, modeling attention as
501 inhibition to inhibitory cells creates the opposite relationship (*i.e.*, a negative
502 correlation) between attentional modulation and normalization. In the 2-D
503 model, any additional inhibitory input to the inhibitory population has the
504 effect of increasing firing rates for many of the cells, even those representing
505 unattended stimuli. The model therefore cannot replicate findings that rely
506 on attention to a non-preferred stimulus causing a decrease in firing rate.
507 This appears to be a consequence of the strong inhibition needed to keep this
508 more complex model in a stable regime. Attention directed toward inhibitory
509 cells also has a surprising effect on the correlations explored in Figure 15. As
510 can be seen in Supplementary Figure A.19E, this fom of attention increases

511 correlations for pairs of cells both with the same and opposite preferred
512 stimuli.

513 *2.6. Attention enhances detection performance in a multi-layer model*

514 An important consequence of deploying attention is enhanced perfor-
515 mance on challenging tasks. We have thus far shown how the SSN can
516 replicate many neural effects of attention, but to truly understand attention,
517 it is necessary to link these neural changes to performance changes. And for
518 that it is necessary to build a functioning model of the visual system that
519 can perform visual tasks.

520 Because the SSN replicates neural findings that have been found in various
521 areas in the visual system, it can be thought of as a canonical circuit, which
522 is repeated throughout the visual hierarchy. To build a biologically-realistic
523 multi-area model of the visual system that can perform a task, we model
524 each area as a set of SSNs, the outputs of which are fed into another set
525 of SSNs (i.e., a downstream visual area). The precise connections between
526 these areas are learned as part of a training procedure. In particular, the
527 SSN circuitry is placed inside a convolutional neural network architecture,
528 creating a model we have dubbed the SSN-CNN (Methods 4.3).

529 The structure of the model can be seen in Figure 16A. The network is
530 a 2-layer convolutional neural network wherein the convolutional filters are
531 constrained to be non-negative (to mimic the excitatory feedforward con-
532 nections that exist between different visual areas). In addition, after each
533 pooling layer is an SSN layer. The SSN layer implements normalization
534 (historically normalization layers have been included in CNNs, typically im-
535 plemented via a divisive normalization equation Krizhevsky et al. (2012)).
536 Specifically, at each 2-D spatial location, a ring SSN implements feature nor-
537 malization across the different feature maps. The recurrent connections of
538 the SSN layers are held constant while all other weights of the network are
539 trained end-to-end via backpropagation through time on the MNIST 10-way
540 digit classification task.

541 After the network is trained on the standard task, the final layer is re-
542 placed by a series of binary classifiers, one for each digit. These binary classi-
543 fiers are trained on digit images to determine if a given digit is present in the
544 image or not (for example, one of the binary classifiers would be trained to
545 classify images as being of the digit '4' or not). To test the impact of atten-
546 tion on the abilities of these binary classifiers, we presented the network with
547 a more challenging task: determining if a given digit is present in an image

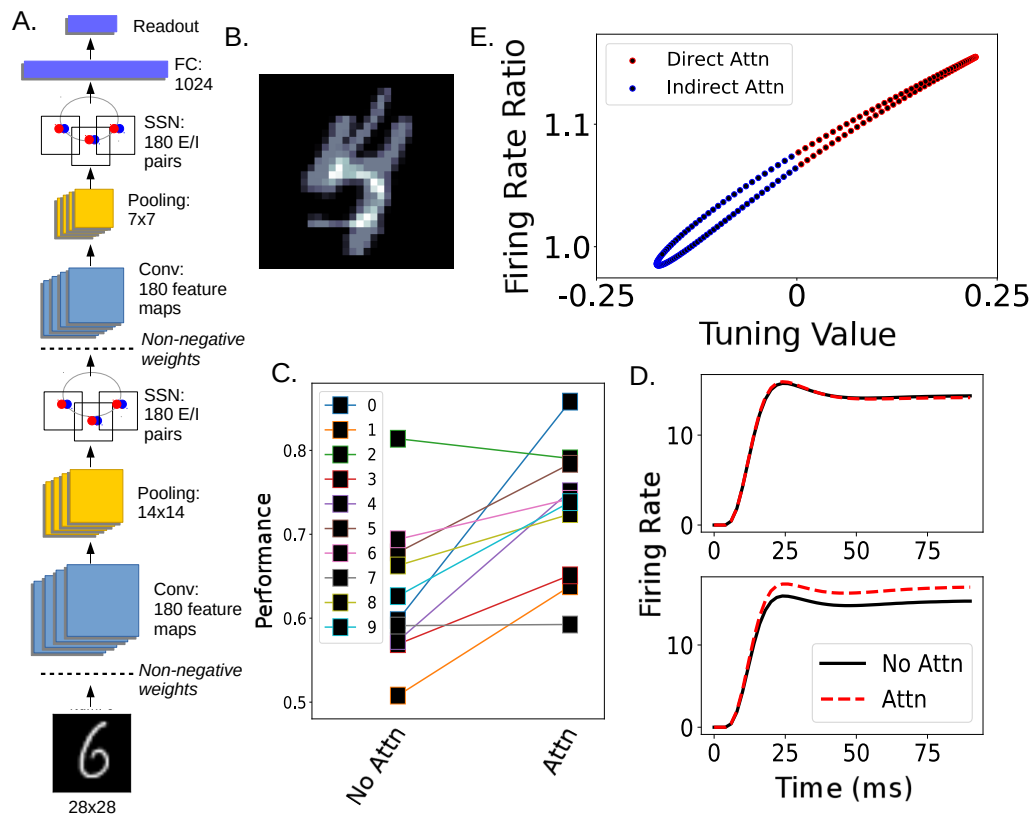


Figure 16:

Attention in the SSN-CNN enhances visual detection performance. A.) The architecture of the SSN-CNN model. In the SSN layers, a full ring model exists at each spatial location (though only one is shown). B.) An example of the images used in the attention task. This image contains a '5' and '4' overlaid, therefore both the binary classifier trained to detect 4s and the one trained to detect 5s should respond positively. C.) Binary detection performance for each digit with (right) and without (left) attention. D.) Example firing rate of two neurons recorded from the second SSN layer with receptive fields at the center of the image when shown the image in (B). The top neuron had a small decrease in firing when attention was deployed to the digit 4 and the bottom had an increase. E.) Impact of attention to the digit 4 on firing rates of excitatory cells (rate with attention divided by rate without) as a function of tuning to the digit. A feature map's tuning value for a given digit is defined as its z-scored mean response to that digit (see Methods, section 4.3). Attention is modeled as excitatory input applied to feature maps whose tuning value is above the median value across maps for that digit. The strength of a map's attentional input is proportional to the difference between that map's tuning value and the median value. Only neurons marked in red were above the median and given direct attentional input.

548 that contains two overlaid digits (Figure 16B). The network performs above
549 chance on this challenging task, and performance increased when attention
550 was applied (Figure 16C, attention applied at layer 2).

551 Attention is applied in this model as previously described: an additional
552 positive input is given to excitatory cells that prefer the attended digit. To
553 determine which cells in the SSN layers “prefer” the attended digit we created
554 tuning curves based on the response of excitatory cells in the SSN when pre-
555 sented with images of different digits (See Methods 4.3). Applying attention
556 in this way still elicits attentional changes in the cells that are not directly
557 targeted—through the recurrent connections—as can be seen in Figure 16E.
558 This includes decreasing the firing rates of neurons that do not prefer the
559 attended digit. While this feature attention is applied the same way across
560 all ring networks at a layer, the pattern of feedforward input will influence
561 the ultimate impact of attention. This can be seen by comparing the ratio of
562 firing with and without attention in ring networks at different nearby spatial
563 locations, which receive slightly different feedforward input (Supplementary
564 Figure A.20).

565 Previous work (Lindsay and Miller (2018); Lindsay (2015)) has shown
566 how attentional changes in different layers of a deep convolutional neural
567 network can lead to enhanced performance on challenging visual tasks. That
568 work demonstrated that the attentional modulation style that works best is
569 multiplicative and bi-directional changes (i.e., the effect of attention should
570 be to scale the activity of neurons that prefer the attended stimulus up
571 and those that don’t prefer it down). What we have shown here is how
572 an additive input solely to the excitatory neurons that prefer the attended
573 stimulus can turn into multiplicative and bi-directional changes via the circuit
574 mechanisms of the SSN and lead to an increase in performance. This allows
575 for a straightforward mechanism by which top-down attentional signals can
576 lead to enhanced performance simply by providing additional synaptic inputs
577 to the right set of excitatory cells.

578 **3. Discussion**

579 The stabilized supralinear network (SSN) is a model of recurrent pro-
580 cessing in visual cortex that is informed by anatomy and replicates several
581 features of neural activity (Rubin et al., 2015). With a simple addition to
582 this nonlinear circuit model, we are able to reproduce a number of exper-
583 imental results on attention in visual cortex (Treue and Martinez Trujillo,

584 1999; Cohen and Maunsell, 2009; Mitchell et al., 2007; Reynolds and Desi-
585 mone, 2003; Sundberg et al., 2009; Lee and Maunsell, 2009; Ni et al., 2012;
586 Martinez-Trujillo and Treue, 2002). Through balanced amplification (Mur-
587 phy and Miller, 2009), a small additional excitatory input to excitatory cells
588 causes a nonlinear scaling of firing rates in a manner consistent with a number
589 of experimental observations. Recurrent connections implement interactions
590 between features and spatial locations. These simple models are able to ac-
591 count for changes in stimulus interactions, differences in gain changes and the
592 magnitude of attention's effects, as well as changes in trial-to-trial variability.
593 We are not aware of any previous model that has attempted to replicate so
594 many effects of attention simultaneously. The ability to replicate all these
595 effects via a small additional input to a subset of neurons provides a simple,
596 plausible mechanism through which higher cortical feedback can implement
597 attention.

598 Previous work has identified areas in the frontal cortex that may be con-
599 sidered the source of top-down selective visual attention (Bichot et al., 2015;
600 Paneri and Gregoriou, 2017). Exactly how connections from these areas
601 target visual areas to create the changes seen with attention is unknown.
602 Studying these feedback connection can be challenging, as it requires de-
603 tailed anatomical investigations across multiple brain areas. For this reason,
604 narrowing the hypothesis space by identifying which mechanisms of feed-
605 back control are theoretically capable of implementing the known effects of
606 attention is important. Here, we show that positive additive input to the
607 excitatory neurons that prefer the attended stimulus can recreate the mul-
608 tiplicative changes observed in both E and I cells and both in cells that
609 prefer and do not prefer the attended stimulus. Adding negative input to
610 the inhibitory cells that prefer the attended stimulus can also replicate most
611 of these effects, except that in our 2D model it tended to raise firing rates
612 of neurons that did not prefer the attended stimulus. We do not know if
613 that is a fundamental problem with a disinhibitory model of attention or if
614 it could be fixed by altering model connectivity. Overall, these results show
615 that feedback connections do not need to be directly responsible for all of
616 the neural effects of attention. Instead, they only need to target a subset of
617 neurons in a simple specific way and the local recurrent circuitry can take
618 care of the rest.

619 There are effects of attention that this model does not readily replicate.
620 For example, spatial attention has been observed to shift and shrink receptive
621 fields. A previous two-layer model with multiplicative attentional inputs

622 and inhibitory recurrent connections was able to replicate these phenomena
623 (Miconi and VanRullen, 2016). Creating a unified model that can capture
624 all of attention’s relevant effects is a goal for future work.

625 In addition to replicating known findings, the set of models presented here
626 can serve as testbeds for future work on attention. In particular, experimental
627 designs can be explored and precise predictions made before carrying out
628 further experiments.

629 Circuit models in neuroscience are frequently built to replicate and under-
630 stand the relationship between anatomy and neural activity. Traditionally,
631 these models do not perform a perceptual or cognitive task. Yet, an ulti-
632 mate understanding of the circuitry of visual perception will need to repli-
633 cate behavioral as well as neural findings. We work towards this goal here
634 by incorporating the SSN model into a convolutional neural network that
635 can perform digit recognition (the SSN-CNN). Through this, we connected
636 the neural changes our model replicates to enhanced detection performance.
637 This model also sets a precedent for how traditional approaches from com-
638 putational neuroscience can be incorporated with the increasingly popular
639 approach of using deep neural networks to study the brain (Yamins and
640 DiCarlo, 2016; Kell and McDermott, 2019).

641 Further connections between neural changes and performance remain to
642 be explored, and the SSN-CNN could be useful in this pursuit. For example,
643 we do not incorporate noise into the SSN-CNN in this work, however using
644 the noisy version of the ring model (Figures 13 and 14) would allow for an
645 exploration of how noise and correlation changes impact performance. We
646 also do not attempt to model or replicate effects of attention on reaction
647 time, however that is possible in this dynamic model. Using the full 2-D
648 model (instead of ring models at each spatial location) would also allow for
649 an exploration of the effects of spatial attention and the interaction between
650 spatial and feature attention.

651 4. Methods

652 Code will be publicly available upon publication.

653 4.1. Basic Circuit Models

654 In this study we employ several different configurations of a basic SSN
655 circuit model, the central unit in all being an interconnected pair of excitatory
656 (E) and inhibitory (I) cells. The two core models are the one-dimensional

657 ring model and the one-dimensional line model. In addition, for Figure 1 we
658 use a simplified 2-cell circuit model, and for Figures 5 and 7 we use a large
659 two-dimensional model.

660 In all models, each neuron, i , is represented as a firing rate unit whose
661 activity, r_i , evolves according to:

$$\tau_i \frac{d}{dt} r_i = -r_i + k ([I_i]_+)^n \quad (2)$$

662 with $n > 1$ (indicating a supralinear activation function). The expression
663 $[v]_+ = \max(v, 0)$, that is, neuronal activity cannot go below zero. The in-
664 puts, I_i , to a given neuron i are comprised of recurrent inputs, feedforward
665 stimulus inputs, and attentional inputs. These inputs and parameter values
666 are specified for each model below. In all models the time constant τ_i has the
667 value $\tau_E = 20$ ms for all E cells and $\tau_I = 10$ ms for all I cells. Simulations
668 are run using the forward Euler method with time step 1ms.

669 All of these models except the E-I pair model were described previously
670 in (Rubin et al., 2015), however we will recap them briefly here. We used all
671 the same model parameters from that study, and did not tune them in any
672 way to get the current results. The models are only modified by the addition
673 of attentional inputs, and by the addition of noise inputs for Figures 13 and
674 14.

675 4.1.1. Ring Model

676 The ring model is intended to represent neurons with a shared retinotopic
677 receptive field but different preferred features. In this model, an E-I pair
678 exists at each location on the ring, with the preferred feature (e.g. orientation
679 or direction) varying smoothly around the ring. The relative input to a cell
680 with preferred orientation θ from a stimulus of orientation ϕ is given by
681 $h(\theta, \phi) = e^{-\frac{d_{circ}(\theta - \phi)^2}{2\sigma_{FF}^2}}$ where $d_{circ}(\theta - \phi)$ is the shortest distance around the
682 circle between θ and ϕ . The absolute stimulus input to a cell comes from
683 multiplying $h(\theta, \phi)$ by the scalar c , which represents the overall strength or
684 contrast of the stimulus. In addition, attention directed towards orientation
685 ϕ' provides extra input to E cells with the same overall shape as a stimulus
686 input, scaled by the attention strength factor, a . (In studies that modeled
687 attention as negative input to I cells rather than positive input to E cells,
688 this input is instead given to inhibitory cells, with $a < 0$.) In total, input to

689 the E or I cell at location θ on the ring is given by:

$$\begin{aligned}
 I_E(\theta) &= ch(\theta, \phi) + ah(\theta, \phi') + \sum_{\theta'} W_{EE}(\theta, \theta') r_E(\theta') - W_{EI}(\theta, \theta') r_I(\theta') \\
 I_I(\theta) &= ch(\theta, \phi) + \sum_{\theta'} W_{IE}(\theta, \theta') r_E(\theta') - W_{II}(\theta, \theta') r_I(\theta')
 \end{aligned}
 \tag{3}$$

690 respectively.

691 Recurrent connections fall off according to $W_{ab}(\theta - \theta') = J_{ab} e^{-\frac{d_{circ}(\theta - \theta')}{2\sigma_{ori}^2}}$,
 692 where $d_{circ}(\theta - \theta')$ is the shortest distance around the circle between θ and
 693 θ' . If multiple stimuli are present the inputs are added linearly.

694 For simulations of this model, the following parameters are used: the
 695 number of E/I pairs is $N = 180$; the spacing in degrees between adjacent
 696 pairs on the ring is $\Delta\theta = 1^\circ$; $J_{EE} = 0.044$, $J_{IE} = 0.042$, $J_{EI} = 0.023$,
 697 $J_{II} = 0.018$, $\sigma_{ori} = 32^\circ$, $\sigma_{FF} = 30^\circ$, $k = 0.04$, $n = 2.0$.

698 The ring and its inputs are schematized in Figure 2.

699 In certain simulations, noise is added to the inputs to these cells. Specifi-
 700 cally, $10 + \nu(\theta, t)$ was added to input to each unit at each timestep. External
 701 noise ν was given by convolution of unit-integral Gaussian temporal filter
 702 (stdev 10 ms) and spatial filter (stdev 8°) with Gaussian spatiotemporally
 703 white noise (mean 0, stdev 40), yielding $\sqrt{\langle \nu^2 \rangle} \approx 1$.

704 4.1.2. Line Model

705 In the line model, each E-I pair represents a different retinotopic location
 706 but all have the same preferred features. Rather than being arranged in
 707 a ring, these pairs are simply placed on a line. The line model follows the
 708 same basic equations as the ring model, however the stimulus input is defined
 709 differently and the recurrent connections are differently arranged.

710 A stimulus input is defined in terms of stimulus center x_0 (taken as zero for
 711 center stimuli), length l and sharpness parameter σ_{RF} . The input to an E-I
 712 pair at location x is given by $s_l(x - x_0) = \left(\frac{1}{1 + e^{-\frac{(x - x_0) + l/2}{\sigma_{RF}}}} \right) \left(1 - \frac{1}{1 + e^{-\frac{(x - x_0) - l/2}{\sigma_{RF}}}} \right)$.
 713 As in the ring model, this input is scaled by the overall strength of the stim-
 714 ulus, c .

715 In this model, there are N E/I units with grid spacing Δx . Recurrent
 716 connections are defined with respect to distance between neurons. Excitatory
 717 projections are given by $W_{aE}(x, x') = J_{aE} e^{-\frac{|x - x'|^2}{2\sigma_{aE}^2}}$ for $a \in \{E, I\}$. Inhibitory
 718 projections W_{aI} are only to the same line position as the projecting neuron.

719 The parameters used in this model are: $N = 101$, $\Delta x = \frac{1^\circ}{3}$, $\sigma_{RF} =$
720 $0.125\Delta x$, $J_{EE} = 1.0$, $J_{IE} = 1.25$, $W_{EI} = 1.0$, $W_{II} = 0.75$, $\sigma_{EE} = \frac{2^\circ}{3}$,
721 $\sigma_{IE} = \frac{4^\circ}{3}$, $k = 0.01$, $n = 2.2$.

722 Again, if multiple stimuli are present their inputs are simply added to-
723 gether and attention takes the same shape as a stimulus but is only directed
724 toward E cells.

725 In one simulation, noise was added to the line model. This noise was
726 similar to that added to the ring model, but with a lower baseline (5 instead
727 of 10) and different spatiotemporal parameters: external noise was given
728 by convolution of unit-integral Gaussian temporal filter (stdev 15 ms) and
729 spatial filter (stdev $3\Delta x$) with Gaussian spatiotemporally white noise (mean
730 0, stdev 10).

731 4.1.3. 2-D Model

732 The one-dimensional ring and line models vary either in preferred retino-
733 topic location or visual feature. To create a model wherein cells have both
734 varying retinotopic as well as feature preferences, we place E-I pairs on a
735 two-dimensional spatial grid representing retinotopy, with an overlaid map
736 of preferred orientation (which may be imagined to represent any circular
737 preferred feature). This model also incorporates randomness in parameters,
738 allowing study of diversity in responses as in Fig. 5.

739 Let $W_{ab}(x, x')$ be the synaptic weight from the cell of type b (E or I), at
740 position x' , with preferred orientation $\theta(x')$, to the cell of type a , at position x ,
741 with preferred orientation $\theta(x)$. Nonzero connections are sparse and chosen
742 randomly, with probability $p(W_{ab}(x, x') \neq 0) = \kappa_b e^{-\frac{(x-x')^2}{2\sigma_{ab}^2}} e^{-\frac{d_{circ}(\theta(x)-\theta(x'))^2}{2\sigma_{ori}^2}}$.
743 Where a nonzero connection exists, $W_{ab}(x, x')$ is chosen randomly from a
744 Gaussian distribution with mean J_{ab} and standard deviation $0.25J_{ab}$; weights
745 of opposite sign to J_{ab} are set to zero. For each cell, the set of recurrent
746 synaptic weights of type b (E or I) it receives are then scaled so that all
747 cells of a given type a (E or I) receive the same total inhibitory and the
748 same total excitatory synaptic weight from the network, equal to J_{ab} times
749 the mean number of connections received under $p(W_{ab}(x, x') \neq 0)$. τ_E , τ_I ,
750 n_E , n_I , and k are also drawn from Gaussian distributions, with standard
751 deviation 0.05 times the mean (parameter values below indicate means).

752 We use a grid of 75×75 E-I pairs. The preferred orientation of an E-I pair
753 is given by a map randomly generated using the method of Ref. (Kaschube
754 et al., 2010), (their supplemental materials, Eq. 20) with $n = 30$ and $k_c =$

755 $\frac{8 \text{ cycles}}{75 \text{ grid intervals}}$. The full map is taken to be $16^\circ \times 16^\circ$; the grid interval
 756 $\Delta x = \frac{16^\circ}{75}$. Boundaries in retinotopic space are periodic. Parameters: $\kappa_E =$
 757 0.1 , $\kappa_I = 0.5$, $J_{EE} = 0.10$, $J_{IE} = 0.38$, $J_{EI} = 0.089$, $J_{II} = 0.096$, $k = 0.012$,
 758 $n_E = 2.0$, $n_I = 2.2$, $\sigma_{EE} = 8\Delta x$, $\sigma_{IE} = 12\Delta x$, $\sigma_{EI} = \sigma_{II} = 4\Delta x$, $\sigma_{ori} = 45^\circ$,
 759 $\sigma_{FF} = 32^\circ$, $\sigma_{RF} = \Delta x$. Degrees can be converted to distance across cortex
 760 by assuming a cortical magnification factor of 0.6 mm/deg, a typical figure
 761 for $5 - 10^\circ$ eccentricity in the cat (Albus, 1975) giving $\sigma_{EE} = \sigma_{IE} = 1.54\text{mm}$,
 762 $\sigma_{EI} = \sigma_{II} = 0.513\text{mm}$, orientation map period 1.2mm.

763 In this model, the relative input to the cell at 2D-position \mathbf{x} with pre-
 764 ferred orientation $\theta(\mathbf{x})$ from a grating of size l centered at position \mathbf{x}' with
 765 orientation ϕ is $h(\mathbf{x}) = s_l(|\mathbf{x} - \mathbf{x}'|)e^{-\frac{d_{circ}(\theta(\mathbf{x})-\phi)^2}{2\sigma_{FF}^2}}$; for a full-field grating, the
 766 relative input is simply $h(\mathbf{x}) = e^{-\frac{d_{circ}(\theta(\mathbf{x})-\phi)^2}{2\sigma_{FF}^2}}$.

767 We used different exponents, $n_I > n_E$, to increase stability despite vari-
 768 ability (as supported by experiments: Supplemental Figure S3 of Ref. Haider
 769 et al., 2010). Variability of τ 's, n 's, k was limited because larger variabil-
 770 ity tended to yield instability; biologically, large variability can probably be
 771 tolerated without instability because of various forms of homeostatic com-
 772 pensation (Turrigiano, 2011), not modeled here.

773 4.1.4. E-I Pair Model

774 In Figure 1 we study an isolated E-I pair. The inputs in this simple
 775 two-neuron model are given by:

$$\begin{aligned} I_E &= W_{EE}r_E - W_{EI} * r_I + c_E \\ I_I &= W_{IE}r_E - W_{II} * r_I + c_I \end{aligned} \quad (4)$$

776 We use the following parameters: $W_{EE} = 1.00$, $W_{IE} = 1.25$, $W_{EI} = 0.75$,
 777 $W_{II} = 0.75$, $k = 0.01$, and $n = 2.2$. The inputs c_E and c_I are the sums of
 778 two components, an ‘‘orientation tuned’’ input that is equal between the two
 779 neurons and an untuned modulatory component added to either the E or I
 780 cell on a given trial. The tuned component is given by a Gaussian curve at
 781 orientation θ : $50e^{-\frac{\theta^2}{2\sigma^2}}$, $\sigma = 20^\circ$. Modulatory input: to I cells, from 0 to 10
 782 in steps of 2.5; to E cells, from 0 to 5 in steps of 1.25.

783 4.2. Attention Experiments

784 Unless otherwise noted, simulations ran for 300ms and final firing rates for
 785 excitatory cells were reported. Attention was modeled as additional input

786 of a specified strength given only to the excitatory cell in a pair. Unless
787 otherwise stated, the shape of the attentional inputs was the same as that of
788 the attended stimulus (as schematized in Figure 4.1.1).

789 *4.2.1. Using the Ring Model*

790 In Figure 3, we used the ring model to show how attention to a non-
791 preferred stimulus enhances suppression. The preferred stimulus was oriented
792 at 45 degrees, with strength 40. The non-preferred was oriented at 135
793 degrees and the strength varied from 0 to 80. Attention was applied to
794 either stimulus at strength 3.

795 In Figure 4, a non-preferred stimulus (oriented at 135 degrees with strength
796 40) for the recorded cell (located at 45 degrees) was present as another stim-
797 ulus (also strength 40) varied from orientation 0 to 180 degrees. Attention
798 (strength 2) was applied to the non-preferred probe stimulus, to the varying
799 stimulus, or not applied at all.

800 In Figure 9 (left), activity was recorded from a cell at 45 degrees while
801 a preferred stimulus (45 degrees) was presented in conjunction with a non-
802 preferred (135 degrees) stimulus. While the non-preferred stimulus remained
803 at strength 50, the strength of the preferred one varied logarithmically from
804 1 to 100. Attention was directed to the non-preferred stimulus with strength
805 5 (or was absent). In Figure 9(right), the contrast of both the preferred and
806 non-preferred stimulus varied logarithmically from $\approx 1-20$. Attention was
807 applied either to the preferred or non-preferred stimulus with strength 1.

808 In Figure 11, the cell located at 10 degrees was recorded. Each combina-
809 tion of a preferred stimulus (20 degrees), intermediate stimulus (60 degrees),
810 non-preferred stimulus (80 degrees), or no stimulus was tested. All stimuli
811 were presented with strength 20 and an additional input of 10 was given to all
812 cells to better match the baseline firing in (Sundberg et al., 2009). Attention
813 (of strength 1.5) was applied to either of the stimuli present or not at all.

814 In Figures 13 and 14, the ring model with added noise was used and
815 simulations ran for 500ms. In Figure 13, for the first 250ms, no stimulus or
816 attentional inputs are given (noise inputs are on throughout). At 250ms, a
817 stimulus of strength 25 located at 90 degrees turns on, and on half of the
818 trials so does an attentional input at the same location (strength 8). 1000
819 trials are run in total. To calculate spontaneous firing rates and Fano factor
820 (FF), firing rates are averaged over 100-250ms. For stimulus-evoked activity,
821 they are averaged over 350-500ms (these are the two epochs compared when
822 calculating the fraction change in firing and FF in the right plot of the figure).

823 Both E and I cells from 30-65 degrees were recorded.

824 In Figure 14, for the first 250ms, no stimulus or attentional inputs are
825 given (noise inputs are on throughout). At 250ms, two stimuli (both of
826 strength 25, one located at 90 degrees and one at 45) turn on, and on half
827 of the trials so does an attentional input at 90 degrees (strength 8). 1000
828 trials are run in total. For the figure on the left, correlations are calculated in
829 overlapping windows of 50ms. On the right, correlations are calculated from
830 firing rates averaged over 350-500ms. E cells at all locations were recorded
831 and correlation is plotted as a function of the distance on the ring between
832 any two pairs.

833 *4.2.2. Using the Line Model*

834 In Figure 6, a stimulus of strength 25 and length $\frac{14}{15}$ spatial degrees was
835 either placed at the center of the receptive field of the cell at position 0,
836 placed in its surround (at a distance of $\frac{21}{15}$ degrees), or placed at both locations
837 simultaneously. In the last configuration, attention (strength 2) was applied
838 either to the stimulus at the center or the surround (or not at all).

839 In Figure 8 (left), a stimulus of length 1 spatial degree is presented at
840 the center of the recorded cell with contrast varying logarithmically from
841 1-100. Attention of strength 1 and length 25 degrees is applied at the same
842 location. For the figure on the right, the size of the attention and stimulus are
843 reversed. To replicate differences in baseline firing shown in (Reynolds and
844 Heeger, 2009), an additional input of 10 is given to all cells in the simulations
845 producing the figure on the left, and an additional input of 2 is given for those
846 on the right.

847 In Figure 10, a stimulus of strength 15 was centered on the receptive field
848 of the recorded cell with length varying from 0 to 2.5 degrees. The size of
849 attention (applied with strength 4) was equal to the length of the stimulus
850 times an attention scale factor which ranged from .3 to 1.2. The preferred
851 length is defined as the length at which the maximal firing rate is elicited.

852 In Figure 12, a stimulus of length 1 degree and strength 25 is centered on
853 the recorded neuron's receptive field. A stimulus of the same size and strength
854 either is or isn't presented in the surround (1.5 degrees away). Attention
855 (strength 1, length 1) is applied to the center or surround location in each
856 condition.

857 In Figure 15, the line model with noise added is used. Two stimuli each
858 of length 2.75 degrees were placed at a distance of 2 degrees on either side
859 of the center of the line model. One had a c of 30 and the other 65. On

860 attention trials, attention was applied to both stimuli with a strength of
861 5. For each ‘recording session’ simulated, excitatory cells 39-63 (roughly 4
862 degrees on either side of the center cell at 51) were recorded as these cells
863 responded to one or the other stimulus alone. Responses to each stimulus
864 alone at $c = 65$ (50 trials each) were used to calculate a d-prime value for
865 each cell that represents the extent to which that cell prefers one stimulus
866 over the other. As in Ruff and Cohen (2014), the product of d-primes defined
867 the TTS (task tuning similarity) value for a pair of cells. 100 attention trials
868 and 100 no attention trials were run to calculate the correlation coefficients
869 for each pair of cells in each condition based on the average firing over the
870 final 25ms of the simulation (results are the same using 250 or 500 trials). 20
871 different ‘recording sessions’ were created using a different random seed for
872 the noise with each one. In addition to the mean changes plotted in Figure
873 15, we also explored the relationship between TTS and correlation by fitting
874 separate lines to the correlation versus TTS plot in the no attention case and
875 the attention case. If attention differently affects negative and positive TTS
876 pairs, the slope of the attention line should be less than the no attention line.
877 Using the same bootstrap analysis as in Ruff and Cohen (2014) we found this
878 to be true for all 20 of our populations (not shown).

879 *4.2.3. Using the 2-D Model*

880 In Figure 5, the two-dimensional model was used to explore the relation-
881 ship between normalization and attention. We sampled 250 excitatory cells
882 from the model. For each cell, a stimulus of preferred orientation, size 16
883 degrees, and strength 40 is presented to the cell. An orthogonal stimulus of
884 the same size, position, and strength (the “null” stimulus) is then presented,
885 and then the preferred and orthogonal stimuli are presented together. At-
886 tention (strength 8) is applied either to the preferred or null stimulus. These
887 response values are used to calculate the normalization modulation index and
888 attention modulation index for each cell.

889 In Figure 7, we sample 100 cells from the model to test the interaction
890 between surround suppression and attention. For each cell, a stimulus of
891 strength of 50 of preferred orientation and size 10 degrees is shown. A stim-
892 ulus with the same orientation and strength is placed in the surround at a
893 distance of 10 degrees, and the response is recorded. The surround at 10 de-
894 grees is, technically, a circumference of possible positions around the center.
895 To decide where to place the surround stimulus, the surrounding neuron at a
896 distance of 10 with a preferred orientation closest to that of the center neuron

897 is chosen. Attention (modulation strength = 5) is then directed either to the
898 center or surround stimulus.

899 *4.3. The SSN-CNN Model and Experiments*

900 The SSN-CNN is an adaptation of a traditional convolutional neural net-
901 work. The inputs to the network are grayscale images of handwritten digits
902 (28-by-28 pixels). The first convolutional layer applies 180 separate 3×3 fil-
903 ters, all of which are constrained during training to contain only non-negative
904 values. The application of these filters results in 180 feature maps, each with
905 a spatial dimension of 28×28 . A 3×3 max-pooling layer with stride 2×2 re-
906 duces the feature map size down to 14×14 . The output of the pooling layer
907 determines the input to the ring SSNs that exist at the next layer. Specifi-
908 cally, at each of the locations on the 14×14 spatial map, there is a ring SSN
909 with 180 E/I pairs. The activity of the units in the 180 feature maps provide
910 the c values (that is, the strength) for inputs centered at that location on
911 the ring. We arbitrarily number the feature maps from 1 to 180 and let ϕ
912 be the number of a particular feature map. Then at spatial position x, y ,
913 the feedforward input to each cell in the E-I pair located at position θ in the
914 ring model is given by $\sum_{\phi} c_{x,y}(\phi) h(\theta, \phi)$, with $c_{x,y}(\phi)$ the activity of the unit
915 in the ϕ feature map in the pooling layer at location x, y , and $h(\theta, \phi)$ the
916 function defined in section 4.1.1. While there is no concept of a ring in the
917 topology of the feature maps prior to learning, we still map the 180 feature
918 maps onto the 180 locations in the ring. Because feature maps assigned to
919 more nearby locations in the ring will more strongly influence one another's
920 output on the ring, the feature maps should ultimately develop structure
921 reflecting the ring topology (Lindsay and Miller, 2018).

922 This architecture is then repeated to create a two-layer convolutional
923 network. The output of the second SSN layer serves as input to a fully-
924 connected layer with 1024 units, which then projects to the final 10-unit
925 layer (one for each digit). For training, the network was unrolled for 46
926 timesteps (with $dt = 2\text{ms}$ for the SSN layers) and trained on the MNIST
927 dataset using backpropagation through time to minimize a cross entropy loss
928 function (batch size 128). Only the final timestep was used for calculating
929 the loss function and classification accuracy. The recurrent weights for each
930 ring SSN at both layers were set as described above for the standard ring
931 network. These weights were not allowed to change during training.

932 Repeating the procedure of (Lindsay and Miller, 2018), once the network
933 was trained on the standard classification task, the final 10-unit layer was

934 replaced with a series of binary classifiers, one for each digit. The weights
935 from the 1024-unit second-to-last layer to the 2-unit final layer were trained
936 to perform binary classification on a balanced training set wherein half of
937 the images were of the given digit and half without.

938 We then generate more challenging images on which to test the benefits
939 of attention. These images consist of two regular MNIST images added
940 together. The test set for each binary classifier contains 768 images, half of
941 which contain (as one of the two digits) the digit the classifier was trained
942 to detect and the other half do not. Performance accuracy is given as the
943 overall percent correct of the binary classifier on this test set.

944 To know how to apply attention, we first present 45 standard MNIST
945 images of each digit to the network and record the activity of neurons in
946 the SSN. From this we calculate “tuning values” that indicate the extent to
947 which each feature map prefers each digit. As in (Lindsay and Miller, 2018),
948 tuning values are defined as a z-scored measure of the feature map’s mean
949 response to each digit. Specifically, for feature map θ in the l^{th} layer, we
950 define $r^l(\theta, n)$ as the activity in response to image n , averaged over all units
951 in the feature map (i.e., over the spatial dimensions). Averaging these values
952 over all images in the training sets ($N_d = 45$ images per digits, 10 digits.
953 $N=450$) gives the mean activity of the feature map $\bar{r}^l(\theta)$:

$$\bar{r}^l(\theta) = \frac{1}{N} \sum_{n=1}^N r^l(\theta, n) \quad (5)$$

954 Tuning values are defined for each feature map and digit, d as:

$$f_d^l(\theta) = \frac{\frac{1}{N_d} \sum_{n \in d} r^l(\theta, n) - \bar{r}^l(\theta)}{\sqrt{\frac{1}{N} \sum_{i=1}^N (r^l(\theta, n) - \bar{r}^l(\theta))^2}} \quad (6)$$

955 When attention is applied to a particular digit, excitatory neurons that
956 prefer that digit are given additional input. Specifically, the cells in feature
957 maps whose tuning value for the attended digit are above the median tuning
958 value for that digit are given attentional inputs. The attentional input to
959 each feature map is proportional to how much above the median its tuning
960 value is:

$$a_d^l(\theta) = \beta(f_d^l(\theta) - \text{median}(\mathbf{f}_d^l)) \quad (7)$$

961 Note, in this model the attentional input to the excitatory cell is fully speci-
962 fied by the above equation (that is, this value is not multiplied by the shape
963 of the feedforward input).

964 We define digit preference on the feature map level (rather than for indi-
965 vidual neurons) because feature attention is known to be a spatially-global
966 phenomenon (that is, attention applied to a particular feature modulates
967 neurons at all spatial locations, (Saenz et al., 2002)).

968 The accuracy on the same test set of overlaid images is again calculated
969 for each digit, now in the presence of attention directed to the digit being
970 detected. An additional parameter representing the overall strength of at-
971 tention (β) is varied (.02, .04, or .06) and for each digit the best performing
972 strength is used.

973 This attention was applied at each SSN layer individually as well as at
974 both together. Here, the results of applying attention at the second SSN layer
975 are reported as this elicited the best performance (a finding that is in line
976 with those reported in (Lindsay and Miller, 2018; Lindsay, 2015), wherein
977 attention at later layers better enhanced performance).

978 5. Acknowledgements

979 We thank Daniel Bear, Aran Nayebi, and other members of Daniel Yamins’s
980 lab for help with the code used to train the SSN-CNN. This work was sup-
981 ported by funding from the Gatsby Foundation, the Sainsbury Wellcome
982 Centre, Google, Marie Skłodowska-Curie Actions, National Science Founda-
983 tion (NeuroNex DBI-1707398), National Science Foundation (IIS-1704938),
984 and the Simons Collaboration on the Global Brain (543017).

985 References

- 986 D. Ress, B. T. Backus, D. J. Heeger, Activity in primary visual cortex
987 predicts performance in a visual detection task, *Nature neuroscience* 3
988 (2000) 940.
- 989 S. Treue, J. H. Maunsell, Effects of attention on the processing of motion
990 in macaque middle temporal and medial superior temporal visual cortical
991 areas, *Journal of Neuroscience* 19 (1999) 7591–7602.
- 992 S. Treue, J. C. Martinez Trujillo, Feature-based attention influences motion
993 processing gain in macaque visual cortex., *Nature* 399 (1999) 575–579.
- 994 M. R. Cohen, J. H. R. Maunsell, Attention improves performance primarily
995 by reducing interneuronal correlations., *Nat Neurosci* 12 (2009) 1594–1600.

- 996 J. C. Martinez-Trujillo, S. Treue, Feature-based attention increases the se-
997 lectivity of population responses in primate visual cortex, *Current Biology*
998 14 (2004) 744–751.
- 999 J. F. Mitchell, K. A. Sundberg, J. H. Reynolds, Differential attention-
1000 dependent response modulation across cell classes in macaque visual area
1001 v4., *Neuron* 55 (2007) 131–141.
- 1002 J. H. Reynolds, D. J. Heeger, The normalization model of attention., *Neuron*
1003 61 (2009) 168–185.
- 1004 J. Lee, J. H. Maunsell, A normalization model of attentional modulation of
1005 single unit responses, *PLoS ONE* 4 (2009) e4651.
- 1006 G. M. Ghose, Attentional modulation of visual responses by flexible input
1007 gain, *J. Neurophysiol.* 101 (2009) 2089–2106.
- 1008 G. M. Boynton, A framework for describing the effects of attention on visual
1009 responses, *Vision Res.* 49 (2009) 1129–1143.
- 1010 M. Carandini, D. J. Heeger, Normalization as a canonical neural computa-
1011 tion, *Nature Reviews Neuroscience* 13 (2012) 51.
- 1012 J. H. Reynolds, R. Desimone, Interacting roles of attention and visual salience
1013 in v4., *Neuron* 37 (2003) 853–863.
- 1014 K. A. Sundberg, J. F. Mitchell, J. H. Reynolds, Spatial attention modulates
1015 center-surround interactions in macaque visual area v4., *Neuron* 61 (2009)
1016 952–963.
- 1017 Y. Ahmadian, D. B. Rubin, K. D. Miller, Analysis of the stabilized supra-
1018 linear network, *Neural computation* 25 (2013) 1994–2037.
- 1019 D. B. Rubin, S. D. Van Hooser, K. D. Miller, The stabilized supralinear
1020 network: a unifying circuit motif underlying multi-input integration in
1021 sensory cortex, *Neuron* 85 (2015) 402–417.
- 1022 G. Hennequin, Y. Ahmadian, D. B. Rubin, M. Lengyel, K. D. Miller, The
1023 Dynamical Regime of Sensory Cortex: Stable Dynamics around a Single
1024 Stimulus-Tuned Attractor Account for Patterns of Noise Variability, *Neu-
1025 ron* 98 (2018) 846–860.

- 1026 Y. Ahmadian, K. D. Miller, What is the dynamical regime of cerebral cortex?,
1027 arXiv preprint arXiv:1908.10101 (2019).
- 1028 B. K. Murphy, K. D. Miller, Balanced amplification: a new mechanism
1029 of selective amplification of neural activity patterns., *Neuron* 61 (2009)
1030 635–648.
- 1031 G. W. Lindsay, K. D. Miller, How biological attention mechanisms improve
1032 task performance in a large-scale visual system model, *eLife* 7 (2018)
1033 e38105.
- 1034 N. J. Priebe, D. Ferster, Mechanisms underlying cross-orientation suppression
1035 in cat visual cortex, *Nature Neurosci.* 9 (2006) 552–561.
- 1036 B. Li, J. K. Thompson, T. Duong, M. R. Peterson, R. D. Freeman, Origins
1037 of cross-orientation suppression in the visual cortex, *J. Neurophysiol.* 96
1038 (2006) 1755–1764.
- 1039 F. Sengpiel, V. Vorobyov, Intracortical origins of interocular suppression in
1040 the visual cortex, *J. Neurosci.* 25 (2005) 6394–6400.
- 1041 H. Ozeki, I. M. Finn, E. S. Schaffer, K. D. Miller, D. Ferster, Inhibitory
1042 stabilization of the cortical network underlies visual surround suppression.,
1043 *Neuron* 62 (2009) 578–592.
- 1044 J. Lee, J. H. R. Maunsell, A normalization model of attentional modulation
1045 of single unit responses., *PLoS One* 4 (2009) e4651.
- 1046 A. M. Ni, S. Ray, J. H. R. Maunsell, Tuned normalization explains the size
1047 of attention modulations., *Neuron* 73 (2012) 803–813.
- 1048 G. Sclar, Expression of “retinal” contrast gain control by neurons of the cat’s
1049 lateral geniculate nucleus., *Exp. Brain Res.* 66 (1987) 589–596.
- 1050 G. Sclar, J. H. Maunsell, P. Lennie, Coding of image contrast in central
1051 visual pathways of the macaque monkey, *Vision Res.* 30 (1990) 1–10.
- 1052 K. I. Naka, W. A. Rushton, S-potentials from luminosity units in the retina
1053 of fish (cyprinidae)., *J Physiol* 185 (1966) 587–599.
- 1054 J. Martinez-Trujillo, S. Treue, Attentional modulation strength in cortical
1055 area mt depends on stimulus contrast., *Neuron* 35 (2002) 365–370.

- 1056 M. Roberts, L. S. Delicato, J. Herrero, M. A. Gieselmann, A. Thiele, Attention
1057 alters spatial integration in macaque v1 in an eccentricity-dependent
1058 manner., *Nat Neurosci* 10 (2007) 1483–1491.
- 1059 J. Lee, J. H. Maunsell, Attentional modulation of mt neurons with single or
1060 multiple stimuli in their receptive fields, *Journal of Neuroscience* 30 (2010)
1061 3058–3066.
- 1062 M. M. Churchland, B. M. Yu, J. P. Cunningham, L. P. Sugrue, M. R. Co-
1063 hen, G. S. Corrado, W. T. Newsome, A. M. Clark, P. Hosseini, B. B. Scott,
1064 D. C. Bradley, M. A. Smith, A. Kohn, J. A. Movshon, K. M. Armstrong,
1065 T. Moore, S. W. Chang, L. H. Snyder, S. G. Lisberger, N. J. Priebe, I. M.
1066 Finn, D. Ferster, S. I. Ryu, G. Santhanam, M. Sahani, K. V. Shenoy, Stim-
1067 ulus onset quenches neural variability: a widespread cortical phenomenon.,
1068 *Nat Neurosci* 13 (2010) 369–378.
- 1069 L. Busse, A. R. Wade, M. Carandini, Representation of concurrent stimuli
1070 by population activity in visual cortex., *Neuron* 64 (2009) 931–942.
- 1071 B. B. Averbeck, P. E. Latham, A. Pouget, Neural correlations, population
1072 coding and computation, *Nature reviews neuroscience* 7 (2006) 358.
- 1073 D. A. Ruff, M. R. Cohen, Attention can either increase or decrease spike
1074 count correlations in visual cortex, *Nature neuroscience* 17 (2014) 1591.
- 1075 S. Zhang, M. Xu, T. Kamigaki, J. P. Hoang Do, W. C. Chang, S. Jenvay,
1076 K. Miyamichi, L. Luo, Y. Dan, Selective attention. Long-range and local
1077 circuits for top-down modulation of visual cortex processing, *Science* 345
1078 (2014) 660–665.
- 1079 Y. Fu, J. M. Tucciarone, J. S. Espinosa, N. Sheng, D. P. Darcy, R. A. Nicoll,
1080 Z. J. Huang, M. P. Stryker, A cortical circuit for gain control by behavioral
1081 state, *Cell* 156 (2014) 1139–1152.
- 1082 X. Jiang, G. Wang, A. J. Lee, R. L. Stornetta, J. J. Zhu, The organization of
1083 two new cortical interneuronal circuits., *Nat Neurosci* 16 (2013) 210–218.
- 1084 M. E. Larkum, The yin and yang of cortical layer 1., *Nat Neurosci* 16 (2013)
1085 114–115.

- 1086 A. Krizhevsky, I. Sutskever, G. E. Hinton, Imagenet classification with deep
1087 convolutional neural networks, in: *Advances in neural information pro-*
1088 *cessing systems*, pp. 1097–1105.
- 1089 G. W. Lindsay, Feature-based attention in convolutional neural networks,
1090 arXiv preprint arXiv:1511.06408 (2015).
- 1091 N. P. Bichot, M. T. Heard, E. M. DeGennaro, R. Desimone, A source for
1092 feature-based attention in the prefrontal cortex, *Neuron* 88 (2015) 832–844.
- 1093 S. Paneri, G. G. Gregoriou, Top-down control of visual attention by the pre-
1094 frontal cortex. functional specialization and long-range interactions, *Frontiers in neuroscience* 11 (2017) 545.
- 1096 T. Miconi, R. VanRullen, A feedback model of attention explains the diverse
1097 effects of attention on neural firing rates and receptive field structure, *PLoS*
1098 *computational biology* 12 (2016) e1004770.
- 1099 D. L. Yamins, J. J. DiCarlo, Using goal-driven deep learning models to
1100 understand sensory cortex, *Nature neuroscience* 19 (2016) 356.
- 1101 A. J. Kell, J. H. McDermott, Deep neural network models of sensory systems:
1102 windows onto the role of task constraints, *Current opinion in neurobiology*
1103 55 (2019) 121–132.
- 1104 M. Kaschube, M. Schnabel, S. Lowel, D. M. Coppel, L. E. White, F. Wolf,
1105 Universality in the evolution of orientation columns in the visual cortex.,
1106 *Science* 330 (2010) 1113–1116.
- 1107 K. Albus, A quantitative study of the projection area of the central and
1108 the paracentral visual field in area 17 of the cat. i. the precision of the
1109 topography., *Exp Brain Res* 24 (1975) 159–179.
- 1110 B. Haider, M. R. Krause, A. Duque, Y. Yu, J. Touryan, J. A. Mazer, D. A.
1111 McCormick, Synaptic and network mechanisms of sparse and reliable vi-
1112 sual cortical activity during nonclassical receptive field stimulation., *Neu-*
1113 *ron* 65 (2010) 107–121.
- 1114 G. Turrigiano, Too many cooks? intrinsic and synaptic homeostatic mecha-
1115 nisms in cortical circuit refinement., *Annu Rev Neurosci* 34 (2011) 89–103.

1116 M. Saenz, G. T. Buracas, G. M. Boynton, Global effects of feature-based
1117 attention in human visual cortex, Nature neuroscience 5 (2002) 631.

1118 Appendix A. Supplementary Figures

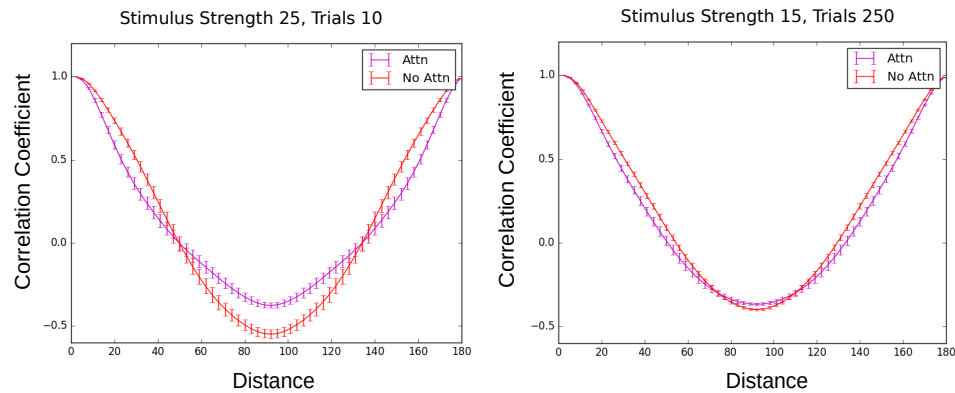


Figure A.17: _____
Attention can increase correlations. Example runs of the model used to make Figure 14 that result in attention increasing correlations for distant pairs. The strength of the stimulus and number of trials used for each condition is given at the top for each (in Figure 14, strength was 25 and 500 trials were used). Errorbars are SEM.

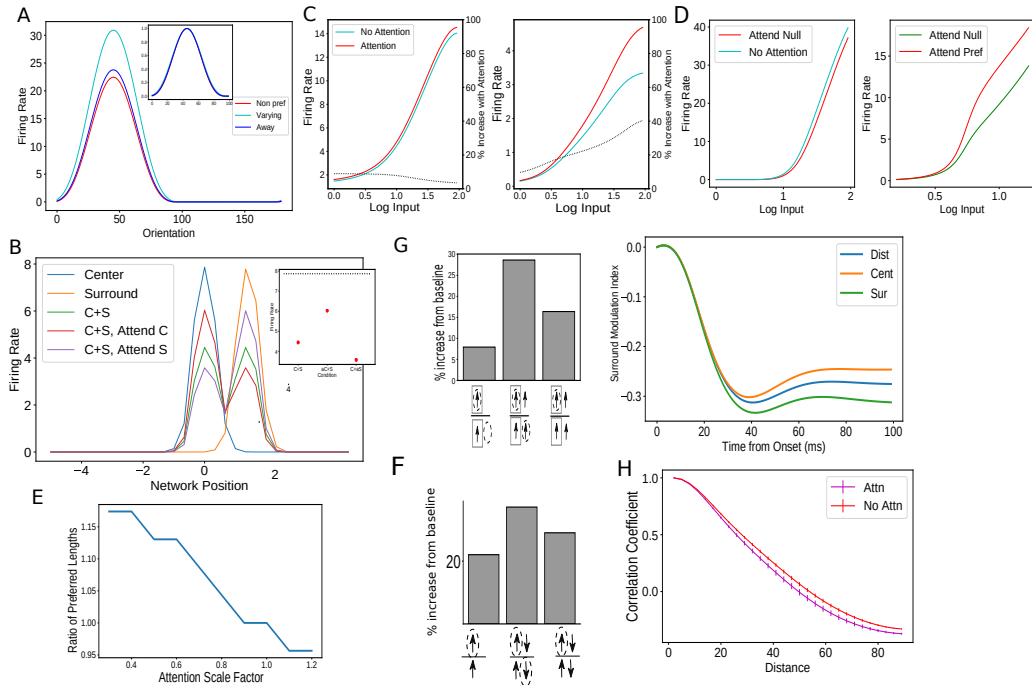


Figure A.18: **Findings that qualitatively replicated with attention modeled as inhibitory input to inhibitory cells** A. Replication of Figure 4. B. Replication of Figure 6. C. Replication of Figure 8. D. Replication of Figure 9. E. Replication of Figure 10. F. Replication of Figure 11. G. Replication of Figure 12. H. Replication of Figure 14.

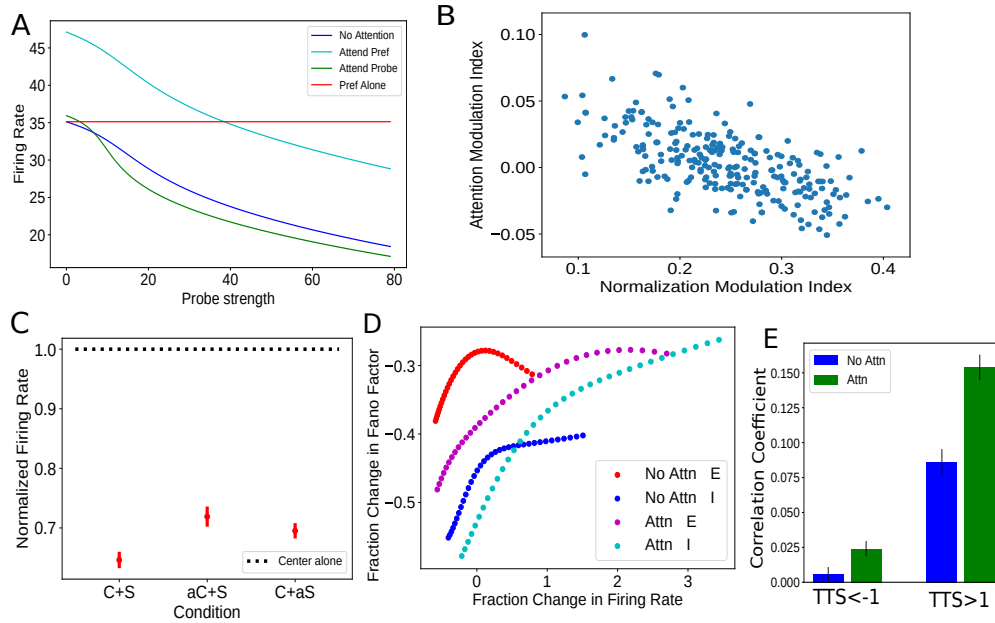


Figure A.19:

Findings not qualitatively replicated with attention modeled as inhibitory input to inhibitory cells A. Figure 3. Here much of the results are replicated however at low probe strengths attending the probe can increase firing rates compared to no attention. B. Figure 5. Here the relationship between normalization and attention is negative. C. Figure 7. Here the attend-surround condition is too similar to the attend-center one. D. Figure 13. Here for a range of firing rate changes, inhibitory cells have their Fano Factor increased with attention (though it should be noted this result happens occasionally when modeling attention as excitation to excitatory cells, for example, when the number of trials is lower). E. Figure 15. Here cell pairs with $TTS_{\neq 1}$ also show an increase in correlation with attention.

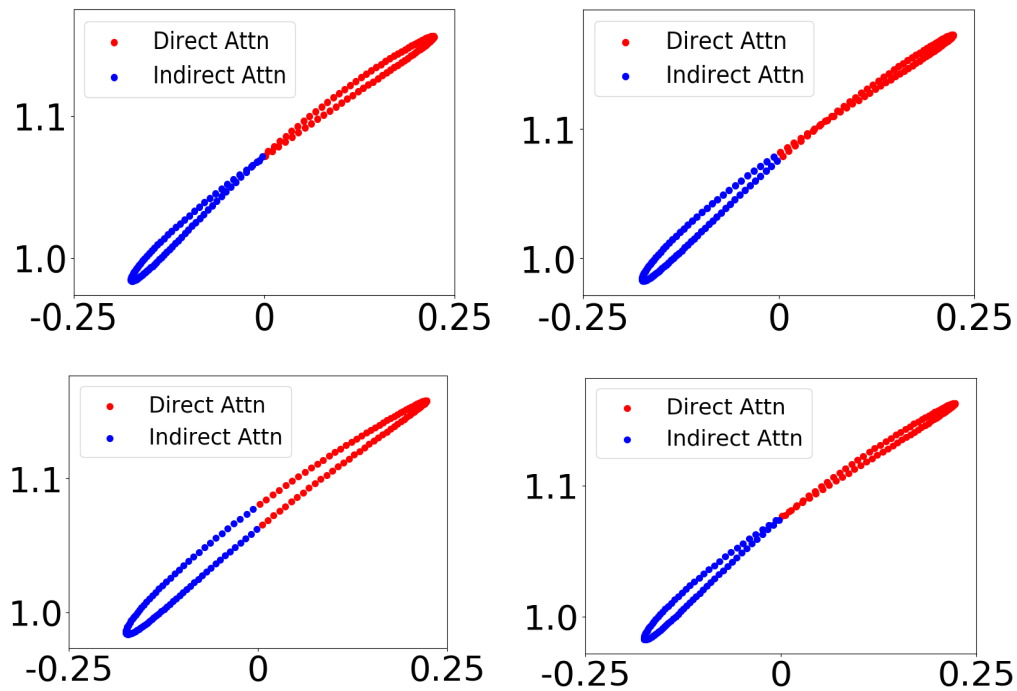


Figure A.20:

Impact of feature attention at different spatial locations in layer 2 of the SSN-CNN Ratio of attended to non-attended firing rates for cells in a ring network as a function of tuning value as in Figure 16E, but for different nearby spatial locations.